UNIVERSITAT POLITÈCNICA DE CATALUNYA
BARCELONATECH
Escola Politècnica Superior d'Enginyeria de Manresa

A PROJECT REPORT ON

DIGITAL TWIN IMPLEMENTATION FOR ELECTRIC MOTOR CONTROL

Final Degree Project

Author: Joan Gomà Rebasa
Degree: Automotive Engineering
University: UPC EPSEM - Escola Politècnica Superior d'Enginyeria de Manresa
Director: Joan Gabriel Bergas Jane
Department: DEE - Departament d'Enginyeria Elèctrica

Abstract

This thesis presents the implementation of a closed-loop control system for an AC brushless motor using a digital twin for development and testing. The purpose of this study is to design a reliable and efficient control strategy that can be used to control a permanent magnet synchronous motor (PMSM) in various applications, such as electric vehicles, robotics, and renewable energy systems.

The first step of this research has been to create a digital twin that simulates the physical system, including the motor, three-phase inverter, power source, and controller, using Simulink. The digital twin has been validated using a set of test signals and the simulation results showed good agreement with the expected behavior of the physical system.

The control algorithm is implemented using Space Vector Pulse Width Modulation (SVPWM) in combination with other mathematical concepts, such as Clake and Parke, to simplify the complexity of the remaining system of equations. Thus, a more efficient control is obtained for both the calculations and commutation of the switches. The SVPWM technique generates a set of voltage vectors applied to the motor to achieve the desired speed and torque. The control algorithm has been optimized to achieve a high efficiency and low harmonic distortion.

Once the simulation has been validated and produces the expected results, the controller code is compiled for deployment. Mencion that the Simulink controller model is the motor control interface, where the variables to be controlled are displayed. The performance of the system is evaluated by measuring the motor speed, torque, and current and comparing the results with the simulation. The experimental results demonstrate the successful implementation of the digital twin, estimation of the motor parameters, and control algorithm. The system achieves good dynamic performance.

In conclusion, the developed control system offers a reliable and efficient control strategy for AC brushless motors, with potential applications in various fields. The digital twin approach provides a flexible and cost-effective way to design and optimize the control system before implementing it in a physical system. The proposed method can be extended to other types of motors and power electronics systems.

Key words:
Digital twin, Parameter estimation (Signal logging and Parameter tuning), Brushless AC Motor control, PMSM, Three phase inverter, Control algorithm implementation, Space Vector Pulse Width Modulation (SVPWM).

Resum

Aquesta tesi presenta la implementació d'un sistema de control de llaç tancat per a un motor AC sense escombretes utilitzant un *digital twin* per al desenvolupament i proves. L'objectiu d'aquest estudi és dissenyar una estratègia de control fiable i eficient que es pugui utilitzar per controlar un motor síncron d'imants permanents (*Permanent Magnet Synchronous Motor*, PMSM) en diverses aplicacions, com ara vehicles elèctrics, robòtica i sistemes d'energies renovables.

El primer pas d'aquesta investigació ha estat crear un *digital twin* que simuli el sistema físic, inclòs el motor, l'inversor trifàsic, la font d'alimentació i el controlador, mitjançant Simulink. El *digital twin* s'ha validat mitjançant un conjunt de senyals de prova i els resultats de la simulació van mostrar un bon acord amb el comportament esperat del sistema físic.

L'algoritme de control s'implementa mitjançant la modulació d'amplada de pols de vectors espacials (*Space Vector Pulse Width Modulation*, SVPWM) en combinació amb altres conceptes matemàtics, com ara Clake i Parke, per simplificar la complexitat del sistema d'equacions restants. Així, s'obté un control més eficient tant per als càlculs com per a la commutació dels interruptors. La tècnica SVPWM genera un conjunt de vectors de tensió aplicats al motor per aconseguir la velocitat i el parell desitjats. L'algoritme de control s'ha optimitzat per obtenir una alta eficiència i una baixa distorsió harmònica.

Un cop validada la simulació i produint els resultats esperats, es compila el codi del controlador per al desplegament. Esmenta que el model de controlador Simulink és la interfície de control del motor, on es mostren les variables a controlar. El rendiment del sistema s'avalua mesurant la velocitat del motor, el parell i el corrent i comparant els resultats amb la simulació. Els resultats experimentals demostren l'èxit d'implementació del *digital twin*, l'estimació dels paràmetres del motor i l'algorisme de control. El sistema assoleix un bon rendiment dinàmic.

En conclusió, el sistema de control desenvolupat ofereix una estratègia de control fiable i eficient per als motors sense escombretes d'AC, amb aplicacions potencials en diversos camps. L'enfocament del *digital twin* proporciona una manera flexible i rendible de dissenyar i optimitzar el sistema de control abans d'implementar-lo en un sistema físic. El mètode proposat es pot estendre a altres tipus de motors i sistemes electrònics de potència.

Paraules clau:
Digital twin, Estimació de paràmetres (Registre de senyal i Afinació de paràmetres), Control de motor AC sense escombretes, PMSM, Inversor trifàsic, Implementació d'algorismes de control, Modulació d'amplada de pols de vector espacial (SVPWM).

List of figures

List of tables

Index

1. Introduction

1.1. Justification of the topic

Electric motor control is a crucial aspect of the industry and condition monitoring plays a vital role in ensuring efficient operation of these machines. Over the years, researchers have developed new techniques and methods for accurately and reliably determining the health of these motors. While classical methods rely on analyzing various machine quantities under stationary conditions, modern methodologies can adapt to any operational regime, including transients. The reliable and efficient operation of electric motors is essential for ensuring the overall productivity, energy efficiency, and safety of many industrial applications.

The early detection of faults or signs of potential failure is one of the most significant challenges in electric motor operation. Conventional motor fault detection methods rely on the analysis of machine quantities under stationary conditions. However, these methods are not always reliable or accurate for identifying faults, particularly under transient operating conditions. Modern methodologies based on transient signal analysis have emerged as promising alternatives. These techniques have proven to be highly effective in detecting faults and have provided significant benefits over conventional approaches, such as a more accurate and reliable determination of the machine's health.

In addition to improving efficiency and reducing energy costs, accurate motor control can also help prevent costly repairs and downtimes. By detecting potential issues early, the system can be shut down before major damage occurs, saving both time and money. Moreover, accurate motor control can improve the safety of the system by ensuring that the motors operate within the safe parameters. This is particularly important in applications in which motor failure can result in hazardous situations.

Therefore, it is crucial to invest in high-quality control systems and monitoring techniques to ensure smooth and efficient operation of industrial motor systems. Real-world examples have shown that these approaches have enormous potential and can offer significant benefits over conventional methods, making them valuable assets for industry.

The latest papers published on this topic show possible advances in incorporating AI and deep learning (DL) in this area. As the National Key Laboratory of Science and Technology on Vessel Integrated Power System, Naval University of Engineering, concludes: “Early detection, isolation, and identification of different faults enabled with DL techniques will help to greatly improve the efficiency, reliability, and repeatability of industrial systems. With the fast development and evolution of DL and related techniques, in near future many fundamental problems, such as the mentioned open challenges, are very likely to be addressed.” [1]

On the other hand, there is a personal motivation and interest in the subject. During these years in the automotive engineering degree, we have studied electronics and control systems, but always from a theoretical point of view. Now, I would like to apply the knowledge learned to a real application, such as the control of an electric motor.

Overall, it has been decided to implement a control algorithm in a physical system. In particular, owing to its recent popularity in power electronics for the automotive sector, it has been decided to control and monitor a three-phase brushless motor.

1.2. Objectives

The objective of this thesis is to implement a closed-loop control system for an AC brushless motor using a digital twin for its development and testing. The purpose of this study is to design a reliable and efficient control strategy that can be used to control a permanent magnet synchronous motor (PMSM) in various applications. To achieve this, a digital twin was designed to first simulate the system and develop a control algorithm. The project objectives have been divided into several goals that represent the development process steps.

The first step is to develop a mathematical model of the permanent magnet synchronous motor (PMSM) system, including a three-phase inverter and controller. The first version of the model represents the studied system in a standard/generic manner. In this step, the theoretical foundations used for the control and parameter estimation are implemented, as well as the modeling of the motor and other physical components.

The resulting models from the previous section are the basis for generating a digital twin of the system to simulate its control with the controller. This would involve simulating the behavior of the motor system using the mathematical model and validating the model against real-world data. The digital twin served as a virtual test bed for the design and tuning of the control parameters. The end result of this section is a Simulink model that simulates the real system, with subsystems for each component.

The next step is to set up the system and tune the control parameters for a specific component of the system. First, the information provided by the manufacturer is used as a first approximation, but because there are no new components, the final parameters will have to be estimated to obtain precise control of the system. However, this part is not included in the controller code. Instead, it is estimated separately and then communicated to the controller.

The control system focuses on achieving stable and accurate speed control of the motor under various operating conditions, and investigates the impact of parameter uncertainties on the performance of the system. Therefore, it is a closed-loop control system.

Once the control parameters are tuned and validated using the digital twin, the next step is to implement the control system on a real three-phase motor system. This involves connecting everything together for a closed-loop control-system configuration. The performance of the real motor system with the implemented control system is validated against the performance predicted by the digital twin. Any discrepancies between the predicted and actual performances would need to be analyzed and addressed.

Overall, the objectives of this thesis are accomplished by using a digital twin approach to design and tune control parameters for a three-phase motor system and to show that the resulting control system can be successfully implemented on a real system with good performance. This thesis would also include an analysis of the limitations and potential future directions for this approach.

1.3. Utility and Scope

This project aims to develop the basis of a control system for electric motors that is sufficiently accurate to implement this control in real applications. Therefore, the project report includes an introduction to the concepts used and a detailed explanation of the control system made with Simulink.

In addition, the control model is presented together with a digital twin that replicates the behavior of the system to be studied. Thus, the control algorithm can be iterated quickly and easily. Using the digital twin approach implies having to model the components in Simulink so that they replicate the behavior of the real system. This means that new models need to be created for other motors or systems.

The final result of this project is a functional control model that applies the aforementioned concepts. The purpose of this memory is for the control to be replicated for the same system or modified to adapt it to new projects. For this, the memory includes the configuration of the blocks used and their utility/function in detail. Besides, by already having a functional control model, it can be improved by considering other phenomena or more motor variables.

2. Development methodology

For this thesis, a step-by-step approach was adopted to achieve the objectives. To acquire a fundamental understanding of the subject, it was divided into simple topics. As research progressed, more intricate issues and concepts were gradually introduced to fulfill the research objectives. The process was iterative and involved regular exercises to progressively comprehend concepts. By implementing this approach, a comprehensive analysis of the research topic was achieved.

Before examining the practical aspects of control systems, it is crucial to establish a firm theoretical foundation. A thorough understanding of the underlying principles and theory of electric motors is key to developing a precise mathematical model that accurately represents the system. Theoretical knowledge lays the groundwork for the effective implementation of control techniques that optimize motor performance while maintaining system stability. Moreover, it was possible to determine the current state of technology and techniques used in the industry.

Additionally, a theoretical understanding of electric motors and control systems enables researchers to identify potential issues and limitations that may arise during the practical implementation phase.

For this process, the recommendations of project director Joan Gabriel Bergas were followed, as well as additional lectures on the subject. Additionally, a search was conducted to collect papers on the topic. This information has been useful for conducting the introductory section 3.Theoretical foundation as well as to understand the necessary elements for the simulation model.

The next step in the analysis of electric motors and control systems involves the development of mathematical models to describe different components of the system. This involves modeling the motor and three-phase inverter, joining the components with the control system, and any other relevant components such as sensors or actuators. The mathematical models are based on the theoretical knowledge gained in the first step and should be sufficiently accurate to enable the simulation and control of the AC motor.

The mathematical models developed in this step will serve as a basis for subsequent steps in the analysis of electric motors and control systems. However, these were used only in the simulation. To control the physical motor, the parameters of the controller and inverter must be indicated in real-time and only the controller model was deployed into the board.

The third step in developing a functional control system is to perform Simulink examples to gain a better understanding of hardware and software interaction. By working with Simulink examples, it can become familiar with hardware software and learn how to develop models and simulations. Simulink is a powerful tool for simulating control systems, and is commonly used in the development of control

systems. It provides a visual interface for developing control algorithms and, if specified, can automatically generate code for the controller.

The following exercises were performed:

- Parameter Tuning and Signal Logging with Serial Communication [2]
- Signal Logging and Parameter Tuning in XCP External Mode with Packed Mode [3]
- Open-Loop Control of 3-Phase AC Motors Using C2000 Processors [4]
- SVPWM Generator (2-Level) [5]

In addition, the information provided by the component manual and laboratory exercises performed in Joan Bergas's lectures has also been very useful.

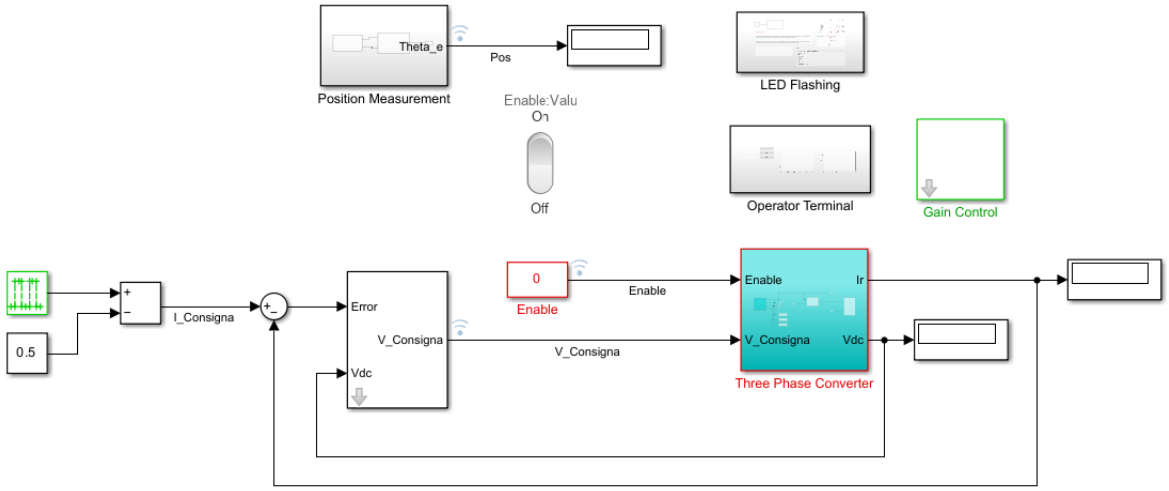

Fig. 1 - Closed-loop control model of a DC motor

Using the knowledge and understanding gained from the previous steps, the next stage is to construct a comprehensive Simulink model that represents the system. This process involves integrating various components of the system, such as the motor, three-phase inverter, and other control system components into the Simulink model. The model should be sufficiently accurate to simulate the behavior of a real-world system while incorporating the control methods studied in the earlier stages. By creating an accurate mathematical representation of the system, control strategies can be designed, tested, and optimized before implementing them in a physical system. This is the main section of the project and is described in detail in section 4.1. Simulation model.

With the Simulink model in place, the next step is to test and experiment in the laboratory. This involves controlling the physical AC motor and collecting data to validate the simulation model. The data collected during the experiment were compared with the simulation model to ensure that the

model accurately represented a real-world system. This step is essential for verifying the accuracy of the simulation model and ensuring that the control system is capable of controlling a real AC motor.

In the final stage of this thesis, conclusions were drawn based on the results obtained from the previous test. This thesis includes a comprehensive discussion of the developed mathematical models, simulation results, and experimental results. Any limitations of the model and experiment are also discussed, along with potential areas for future research and their environmental implications. By analyzing and discussing the results, it provides insights into the design and development of effective control systems for electric motors, as well as their impact on the environment.

3. Theoretical foundation

This section explores the theoretical mathematical foundations of controlling a three-phase motor system. These foundations are divided into several key concepts and theories, including three-phase systems, electromagnetic theory, control theory, signal processing, and optimization.

Three-phase systems utilize three alternating current voltages out of phase with each other at 120º to generate a rotating magnetic field, which drives the motor's rotor. For the control algorithm, electromagnetic theory is vital for accurately modeling the behavior of a motor system and, in particular, for determining how a three-phase PMSM operates. Moreover, digital twin technology involves the use of mathematical models to create a virtual replica. This thesis focuses on the control of the physical system, so it will not go into details of electromagnetic theory, and existing mathematical models will be used for the simulation (9.1. Annex 1: PMSM mathematical model).

Control theory is used to design algorithms that control the motor speed, torque, and position. For this algorithm, Space Vector Pulse Width Modulation is implemented, which is the industry standard method of modulation, in addition to all the necessary transformations. The SVPWM technique can provide precise control over the speed and torque of the electric motor and improve the efficiency and reliability of the system. This is the main content of the section, and is explained in more detail below.

Combining these concepts and theories, the goal is to create a comprehensive model of the motor system that accurately reflects its behavior and to use the model to design control algorithms to optimize performance. The following diagram exemplifies the algorithm that is to be achieved.

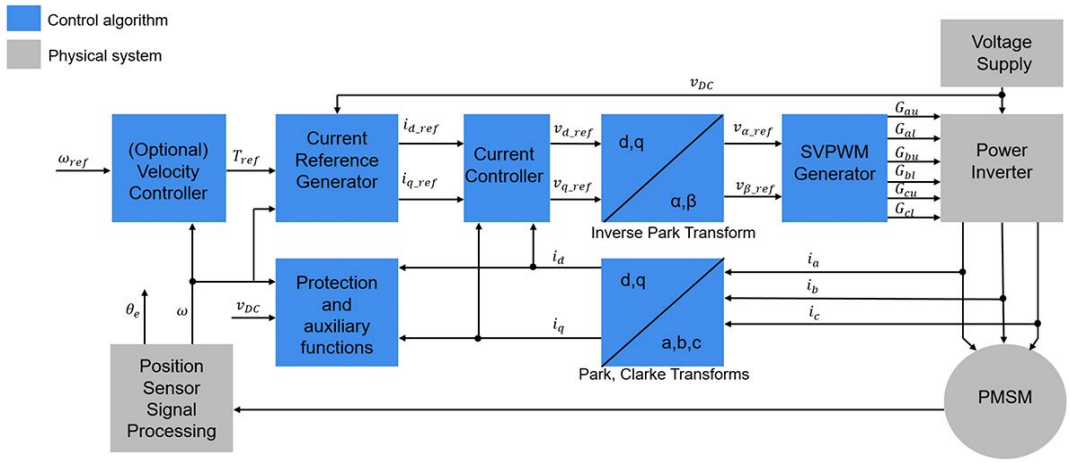

Fig. 2 - Field Oriented Control Block Diagram [6]

3.1. Clark transformation

To maximize the torque produced in a brushless motor, the induced magnetic field should be perpendicular to and ahead of the magnetic field of the rotor. When it comes to measurement and control, considering the current flowing through phases is a simpler approach than focusing on the generated magnetic fields. Therefore, the concept of having a coil of wires that generates a magnetic field in the same direction as the current has been used.

Because these three-phase current and magnetic field vectors can be described on a two-dimensional plane, it is possible to describe the result as a 2d vector and then, it can be theoretically possible to generate any equivalent resultant vector from just two phases, which is the idea behind the Clark transformation.

The Clark transform describes the movement from the *abc* windings to the *alpha-beta* frame. This transformation can largely derive geometrically, considering that *a* point is strictly in the *alpha* direction and *b c* process as it shows the following matrix equation.

$$\begin{bmatrix} i_\alpha \\ i_\beta \end{bmatrix} = \frac{2}{3}\begin{bmatrix} 1 & -\cos(60) & -\cos(60) \\ 0 & \sin(60) & -\sin(60) \end{bmatrix}\begin{bmatrix} i_a \\ i_b \\ i_c \end{bmatrix} = \frac{2}{3}\begin{bmatrix} 1 & -\frac{1}{2} & -\frac{1}{2} \\ 0 & \frac{\sqrt{3}}{2} & -\frac{\sqrt{3}}{2} \end{bmatrix}\begin{bmatrix} i_a \\ i_b \\ i_c \end{bmatrix}$$

The Clark transform also includes an external two-thirds multiplier, which keeps the vectors equal in magnitude on either side of the transformation. To run 1 A from right to left through a three-phase diagram, it must come out of *b* and *c* in equal proportions, assuming that the system obeys Kirchhoff's current law. Thus, two-thirds of the current represented by the summation of the *abc* frame must be taken to obtain 1 A.

However, it can be further simplified by assuming the system to be balanced and thus follows Kirchhoff's current law:

$$i_\alpha = i_a \;\; ; \;\; i_\beta = \frac{i_b - i_c}{\sqrt{3}}$$

Now, we can describe the direction of the current and the induced magnetic fields using the *alpha* and *beta* axes.

3.2. Park transformation

Moreover, torque is produced by a magnetic field perpendicular to the rotor's magnetic field, whereas induction along the direction of the rotor's magnetic field results in it being either amplified or weakened when it sums up with the rotor's magnetic field. The equivalent induction of a three-phase motor can be described in two directions, as shown above, and this representation can be analyzed from the perspective of the rotor. This analysis can be performed using what is known as Park transformation, which involves creating another reference frame that rotates with the rotor. By convention, the axes of this frame are referred to as the direct or *d* axis and quadrature or *q* axis. The direct axis points in the direction of the rotor's magnetic field, while the quadrature axis is located 90° counterclockwise.

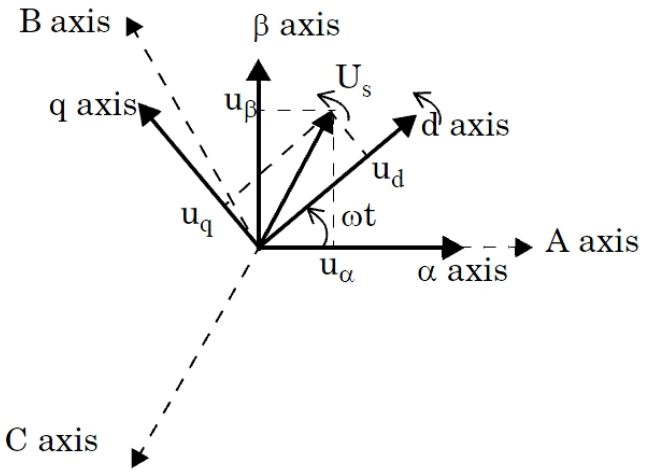

Fig. 3 - *Alpha-Beta-Zero* to *dq0* frames [7]

Therefore, a magnetic field induced in the positive *q* direction produces a counterclockwise torque, whereas that induced in the negative *q* direction produces a clockwise torque. Whereas a magnetic field induced in the positive *d* direction corresponds to strengthening the magnetic field of the rotor, an induction in the negative *d* direction weakens the field of the rotor.

Because the *dq* axis maintains the same origin as the *alpha-beta* axis, the transformation between the two can be described as a simple rotation matrix. Note that *θ* is the angle between *alpha* and *d*.

$$\begin{bmatrix} i_d \\ i_q \end{bmatrix} = \begin{bmatrix} \cos(\theta) & \sin(\theta) \\ -\sin(\theta) & \cos(\theta) \end{bmatrix} \begin{bmatrix} i_\alpha \\ i_\beta \end{bmatrix}$$

To optimize the amount of torque obtained per current in a non-salient-pole motor, it is desired that the current strictly points in the *q* axis direction. A six-block commutation scheme can be used to achieve this, starting from the center of Hall sector 0 and connecting the appropriate phases using a diagram. Initially, when aligned with the *q* axis, the motor optimally generates torque. However, during movement across the remainder of this Hall sector, the current direction is no longer aligned with the *q* axis. As a result, the current direction oscillates up and down, and a torque ripple is created as it approaches the edges of the Hall sectors.

As mentioned earlier, the current and magnetic field vectors are required to point in the *q* direction. When only two phases are connected at a time, as in the six-sector block commutation, generating a vector in this direction is not possible. However, by independently controlling each motor phase with a three-legged h-bridge, the limitation of connecting only two phases at a time was removed. Thus, by connecting node *b* to the ground and nodes *a* and *c* to a high voltage, vectors pointing strictly in the *q* direction can be generated for this orientation. For each of the six new Hall sectors added by the new sensors, the current can be aligned with the *q* axis by connecting either two phases to high and one to ground or two phases to ground and one to high.

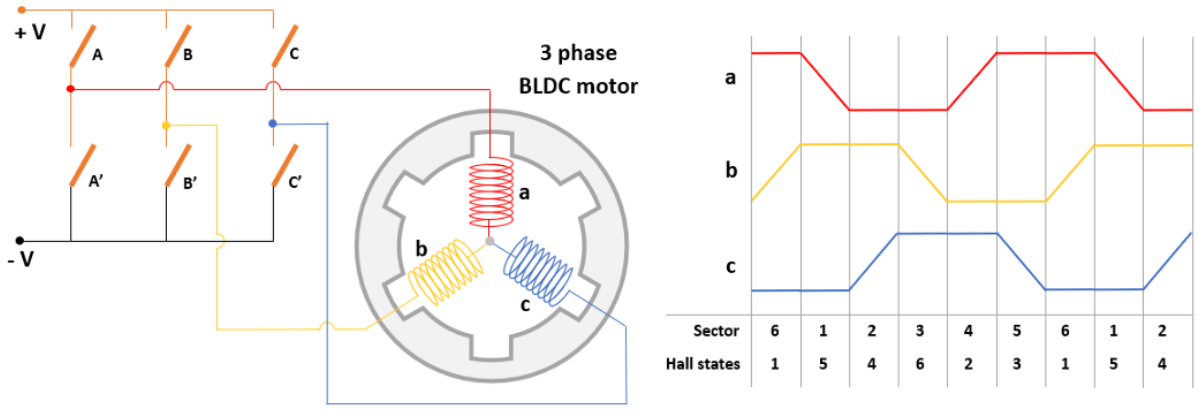

Fig. 4 - Six Step commutation diagram [8]

When more than two phases are connected at 100% duty cycle, other side effects can be observed on the current and torque ripples. As will be seen, the individual phases of the motor can be electrically represented as a load consisting of a resistor, an inductor, and a back emf.

When two phases are connected, as was done with six-sector block commutation, the values of the resistors and inductors of the two phases increase, as they are in series with each other. However, if all three phases are utilized, two of them will be parallel to each other and then in series with the remaining phase. Thus, by using three phases instead of two, the amount of resistance and inductance experienced by the current decreases.

It may appear that by applying 33% more current, it is possible to generate 33% more torque. However, upon examining the summation of vectors, it becomes evident that when all three phases are utilized, the parallel phases cancel out. As a result, although 33% more current runs through the system, only approximately 15% more net magnetic flux is obtained because a larger portion of the vector is canceled along the *d* axis. However, more torque could still be generated in these configurations.

Because Kirchhoff's current law is followed by this system, all three currents cannot be arbitrarily defined. Instead, the currents exiting *a* and *b* are defined as functions of *theta*, where theta equals zero and corresponds to the *d* axis being aligned with the *alpha* axis.

$$
\begin{aligned}
i_a &= -i \cdot \sin(\theta) \\
i_b &= -i \cdot \sin(\theta - 120) \\
i_c &= -i \cdot \sin(\theta + 120)
\end{aligned}
$$

$$
\begin{aligned}
i_\alpha &= i_a = -i \cdot \sin(\theta) \\
i_\beta &= \frac{i_b - i_c}{\sqrt{3}} = i \cdot \cos(\theta)
\end{aligned}
$$

If the part transformation is carried out and moved into the *dq* reference frame, it can be observed that the currents in the *d* direction are all canceled out, and the current in the *q* direction remains constant.

$$
\begin{aligned}
i_Q &= -\sin(\theta) \cdot i_\alpha + \cos(\theta) \cdot i_\beta = i \cdot \left(\sin^2(\theta) + \cos^2(\theta)\right) = i \\
i_D &= \cos(\theta) \cdot i_\alpha + \sin(\theta) \cdot i_\beta = i \cdot (\cos(\theta)\sin(\theta) - \sin(\theta)\cos(\theta)) = 0
\end{aligned}
$$

This indicated that the torque ripple was completely eliminated. The current plot for each of the three reference frames is shown below. To simplify the schematic, these results were obtained from Simulink using Simscape blocks. Therefore, it can be observed that if the current waveforms from block commutation are replaced with sinusoidal currents, torque ripple can be minimized, and the *d* axis current can be driven to zero. However, this is only intended as a quick example to help understand the transformations that are performed. Simscape blocks are not used in the control code.

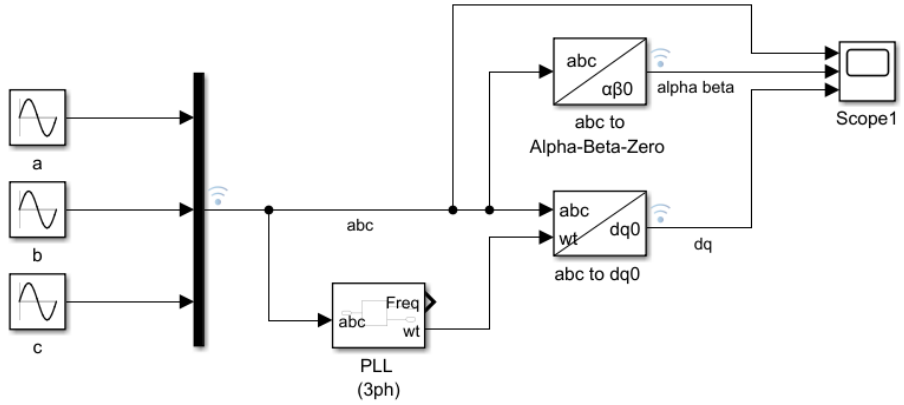

Fig. 5 - Clarke and Park transformation example using Simscape blocks

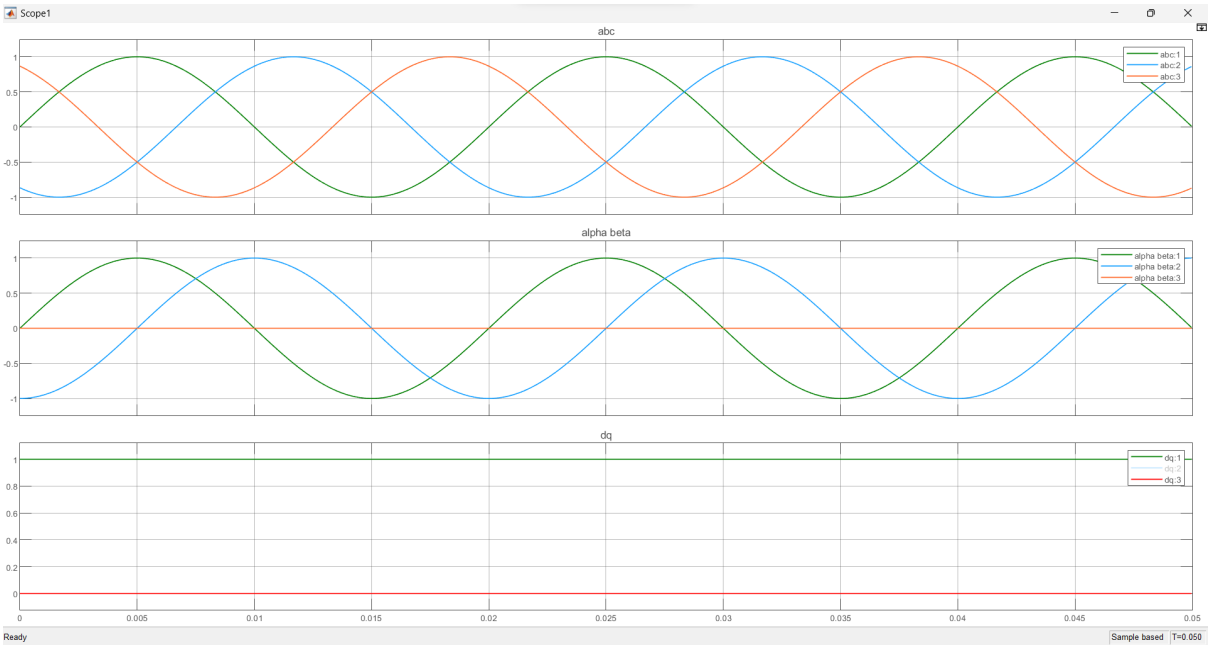

Fig. 6 - Clarke and Park transformation current [A] example output (Scope1)

3.3. Space Vector Pulse Width Modulation

The industry standard method of modulation, which takes full advantage of the supply voltage, is voltage Space Vector Pulse Width Modulation that rotates with the motor angle to stay in line with the *q* axis. In the previous sections, a method for producing a smooth and optimized torque in a motor was developed, and the optimal modulation method arrived at is the alternate reverse space vector modulation pattern. SVPWM is a technique used in modern inverters to control the speed and torque of AC motors efficiently. In the SVPWM, the reference voltage is transformed into a space vector, which is then compared with the voltage generated by the motor. The resulting error signal is used to generate the switching signals for the inverter.

SVPWM has several advantages over other PWM techniques, including a higher efficiency, lower harmonic distortion, and faster dynamic response. It also allows for precise control of motor speed and torque, making it an ideal choice for many industrial applications. [9]

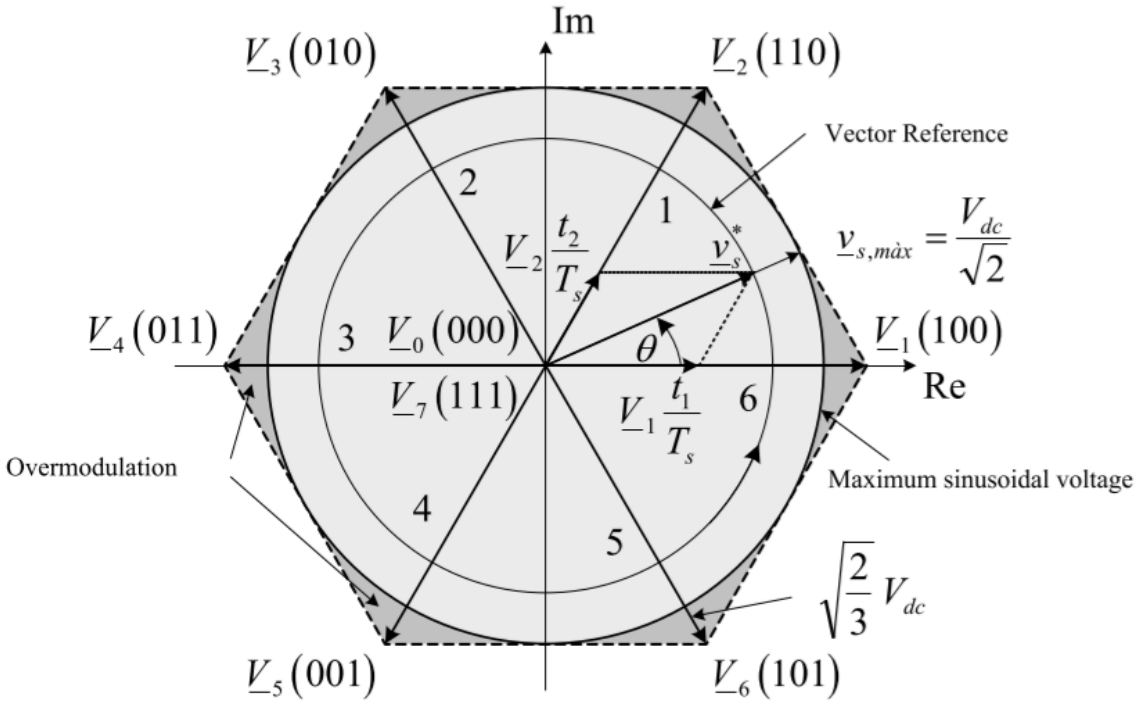

Fig. 7 - Space Vector Pulse Width Modulation [10]

During space vector modulation, all three phases must be constantly connected to either high voltage or ground, and six configurations involving all three phases are used to drive the current, each pointing to a unique and discrete angle. To produce a voltage vector that continuously turns with the rotor, the forced phase of the PWM period is subdivided into t_1 and t_2.

During t_1, the voltage configuration that produces the field vector closest to the desired vector in the clockwise direction is applied, whereas during t_2, the voltage configuration that produces the vector closest to the desired vector in the counterclockwise direction is applied. The duration of t_1 relative to t_2 is determined by the desired vector orientation relative to the vectors generated by the two chosen voltage configurations.

$$T_{aon} = t_0/2 \qquad T_{aoff} = t_0/2 + t_1 + t_2$$
$$T_{bon} = t_0/2 + t_1 \qquad T_{boff} = t_0/2 + t_2$$
$$T_{con} = t_0/2 + t_1 + t_2 \qquad T_{coff} = t_0/2$$

$$\begin{bmatrix} T_{aoff} \\ T_{boff} \\ T_{coff} \end{bmatrix} = \left[\begin{array}{ccc|ccc|ccc|ccc|ccc|ccc} \multicolumn{3}{c|}{\text{sector 1}} & \multicolumn{3}{c|}{\text{sector 2}} & \multicolumn{3}{c|}{\text{sector 3}} & \multicolumn{3}{c|}{\text{sector 4}} & \multicolumn{3}{c|}{\text{sector 5}} & \multicolumn{3}{c}{\text{sector 6}} \\ 1 & 1 & 1 & 1 & 1 & 1 & 1 & 1 & 1 & 1 & 1 & 1 & 1 & 1 & 1 & 1 & 1 & 1 \\ 1 & 0 & 0 & 1 & 1 & 0 & 0 & 1 & 0 & 0 & 1 & 1 & 0 & 0 & 1 & 1 & 0 & 1 \\ 1 & 1 & 0 & 0 & 1 & 0 & 0 & 1 & 1 & 0 & 0 & 1 & 1 & 0 & 1 & 1 & 0 & 0 \end{array}\right]^T \begin{bmatrix} t_0/2 \\ t_1 \\ t_2 \end{bmatrix}$$

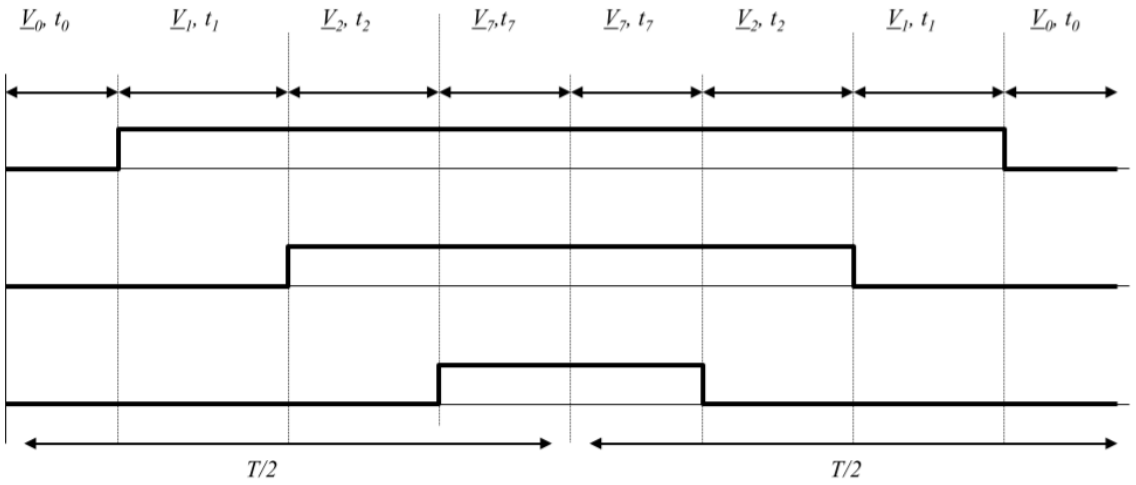

Fig. 8 - Commutation table SVPWM [10]

During the unforced phase of the PWM period, at least one of two "null voltage configurations" is used while performing space vector modulation, involving all three phases connected to high voltage or all three phases connected to low voltage. These two configurations are referred to as voltage configuration 0 and voltage configuration 7.

The alternate reverse sequence, which has less harmonic distortion, uses both, evenly splitting its unforced phase between them. Generally, with space-vector modulation patterns, PWM signals generally need to be center-aligned.

SVPWM is used in conjunction with the Park transformation because it allows precise control of the motor's output. In particular, SVPWM allows for control of the motor's voltage and current waveforms, which can be used to control the motor's speed and torque. It is also true that it is impossible to return from *dq0* to the *abc* axes, which is another reason why SVPWM is required when performing the Park transformation. The transformation from *abc* to *dq0* is a one-way transformation, which implies that it cannot be undone. SVPWM allows for precise control of the motor's output in the *dq* frame, which is where control algorithms are typically implemented [10].

By modifying the previous example, a block that performs the necessary calculations to obtain the commutation of the switches starting from alpha and beta can be incorporated: SVPWM Generator (2-Level) from the Simscape library. To visualize the result, the states of the switches have been grouped in pairs, such that if one is on and the other is off. Figure 10 shows this phenomenon, in which the time on varied throughout the simulation. The simulation time has been reduced to 0,005 s.

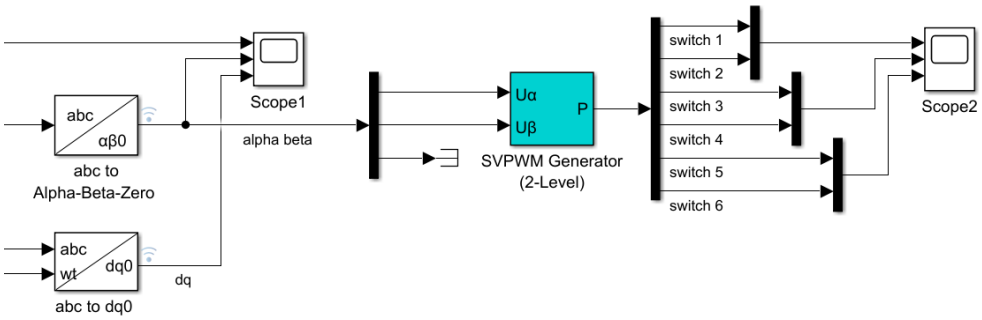

Fig. 9 - SVPWM example using Simscape blocks

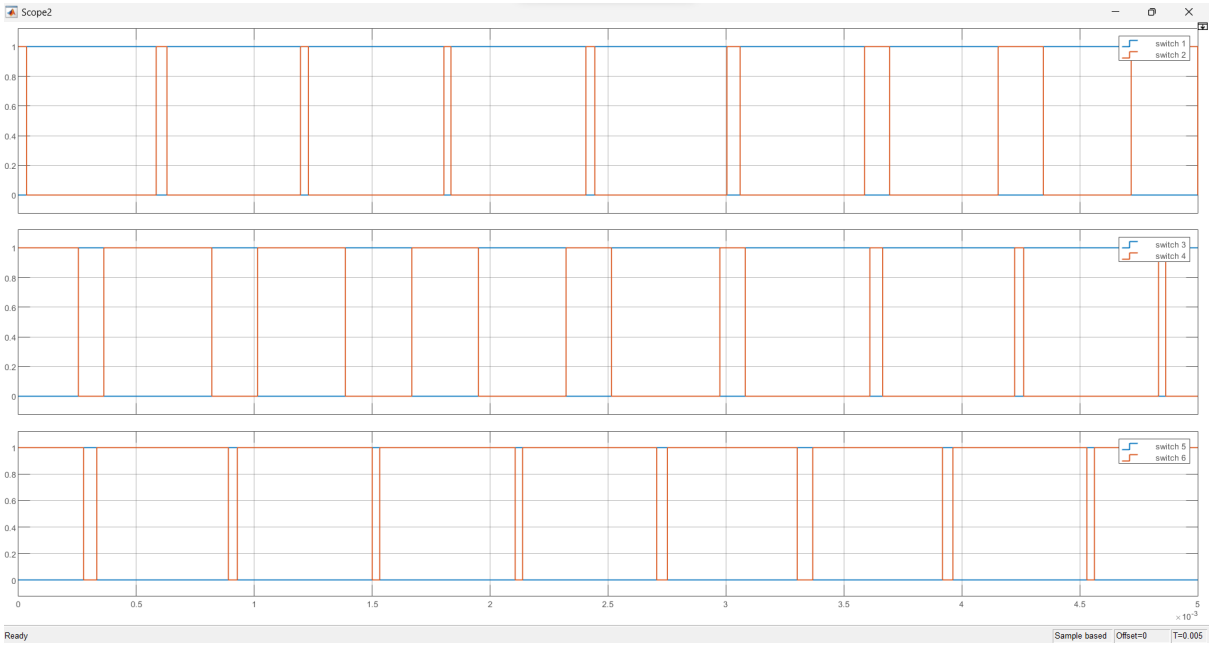

Fig. 10 - SVPWM example output (Scope2)

4. System modeling

4.1. Simulation model

This section provides a detailed explanation of the simulation's various components and the control algorithm. Simulink was used to model the physical system and generate the controller code.

The goal is to develop an effective control system that can regulate motor speed under various operating conditions, such as different loads. The Simulink model functions as a digital counterpart of the physical motor system, enabling experimentation and verification of different control approaches in a simulated setting. Consequently, certain components are represented twice: a model for simulation and another for code generation. This is because specific libraries and packages are required to generate the code and deploy it in the controller. Others are not necessarily included in the code generation, as is the case with the motor, which is only needed in the simulation.

The AC motor control system consists of several components, including the motor and inverter, as well as sensors that measure the current and voltage of the motor. A feedback loop is used to monitor motor performance and regulate control signals accordingly. In addition, a control interface is included, which allows for the adjustment and fine-tuning of the specified system parameters. The system was designed to use a PID controller to regulate the motor's speed and torque based on feedback signals from the sensors.

The Simulink model allows for the simulation of diverse operating conditions, such as changes in the load of the motor and the evaluation of the performance of the control system under these conditions. In addition, the model enables the testing of different control strategies to optimize the performance of the motor under various operating conditions. Nonetheless, in this instance, SVPWM was implemented as previously stated.

The Simulink model is based on the Code Generation template format, which shows how to start code generation using plant and controller models. Furthermore, the controller settings were optimized for code efficiency. The entire model is connected to the feedback_harness.slx file that links the controller and plant. The following sections explain the characteristics of each model in detail.

4.1.1. Harness

The harness connects both models, representing the physical system in the Controller and Plant. However, this presents several problems. On the one hand, the Controller model is designed to be compiled and deployed in the real controller. This means that the model will run in discrete time and use single-precision variables (stored as 4-byte (32-bit) floating-point values of data type (class) single). For this reason, the simulation of the controller is carried out in Fixed-step with a discrete (non-continuous states) solver. In a discrete-time simulation, the system is modeled as a sequence of time steps, where the state of the system is updated at each time step. The time steps are fixed and equally spaced; in this case, the fundamental sample time is 0,00001 s.

On the other hand, the Plant will simulate in continuous time and will use double data type, which is the default numeric class in Simulink. It provides sufficient precision for most computational tasks (8-byte double-precision floating point values). Using a continuous-time simulation implies that the system is modeled as a set of differential equations that describe how the state of the system changes over time. In a continuous-time simulation, time is treated as a continuous variable and the state of the system is updated continuously (not every fixed time, such as the Controller).

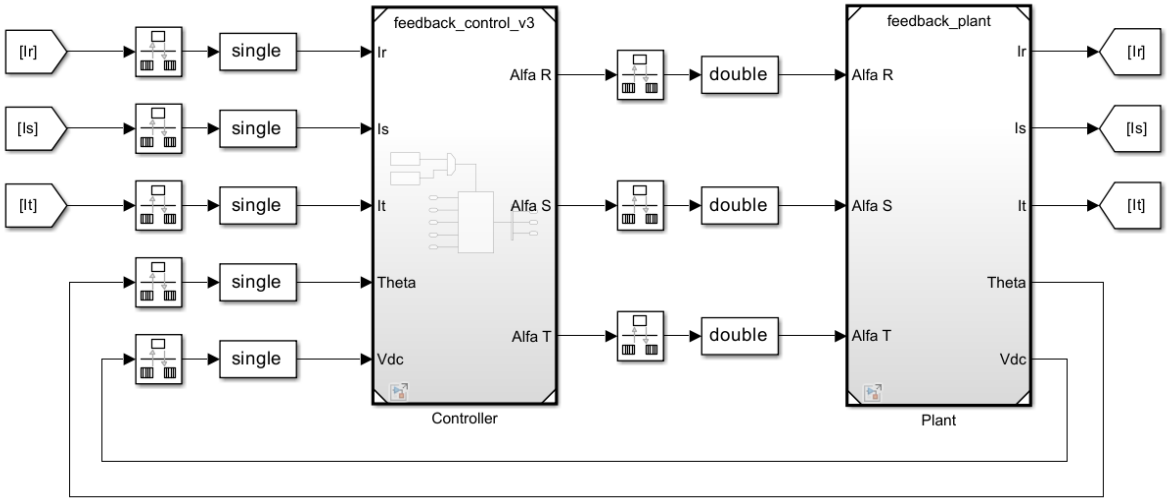

Fig. 11 - Harness, system representation

This is only an inconvenience for the simulation, since both models must communicate, while for code generation only the controller model is used. For this reason, it has been decided to convert data types in the harness.

RT and Data Type Conversion blocks are used to solve this problem. The Rate Transition block transfers data from the output of a block operating at one rate to the input of a block operating at a different rate. On the other hand, the Data Type Conversion block converts the input signal of any Simulink data type to the specified data type. This conversion can also be specified in the inputs and outputs of the system, although by using blocks, the conversion can be easily visualized.

4.1.2. Controller

The controller model must work in both the simulation and code generation. On one hand, it must perform all the necessary calculations to simulate the behavior of the real controller. Therefore, the model should have the same inputs and outputs and perform equivalent calculations.

On the other hand, the same model will be used to generate the code that will be executed in the controller. The Embedded Coder® Support Package for Texas Instruments™ C2000™ Processors addon was used for this project. This makes it possible to generate a real-time executable and download it to a TI development board. The Embedded Coder automatically generates C code and inserts I/O device drivers in the block diagram.

Note that in the case of generating code, only the controller is considered, not the harness of the entire system. Simulink allows for easy differentiation between the two options when using Variant Source/Sink blocks and simplifies the final code or simulation by turning off unused blocks.

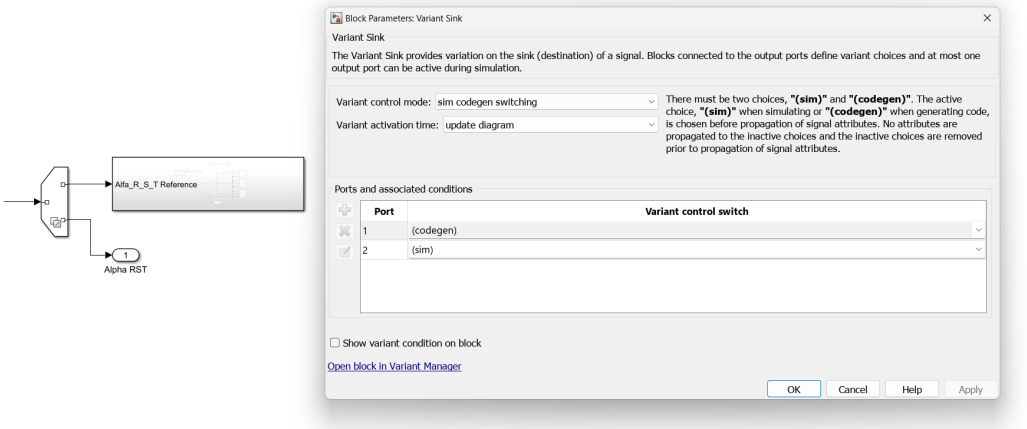

Fig. 12 - Variant Sink block parameters

The controller model consisted of the following elements, each represented in a subsystem:

- A timer interrupt (IRQ) that allows asynchronous processing.
- The ADC Channels, which read actual information from the system.
- The Position Measurement, which uses the motor encoder to calculate its position.
- The Brushless controller subsystem, which performs the necessary calculations to make the motor work.
- The inverter subsystem that sends the signal to the real three-phase inverter.

4.1.2.1. ADC Interrupt

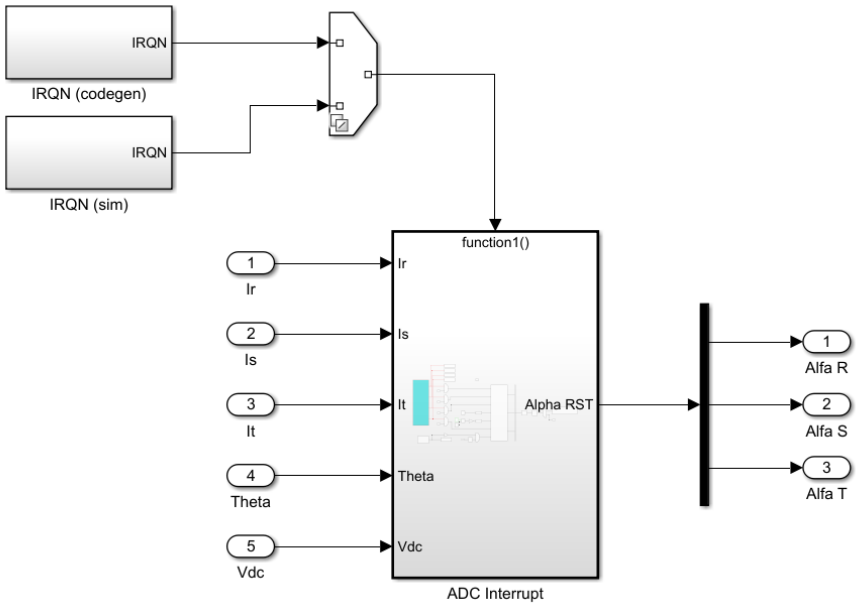

Fig. 13 - Controller first layer

To begin with, execution scheduling models based on timer interrupts do not meet the requirements of some real-time applications to respond to external events. The C28x Hardware Interrupt block addresses this problem by allowing the asynchronous processing of interrupts triggered by events managed by other blocks in the C28x DSP Chip Support Library.

In this case, the block that activates the interrupt is the ADC, which reads the current that passes through the three phases and voltage (external event). When the interrupt is activated, the ADC Interrupt subsystem code is executed with input from the function block.

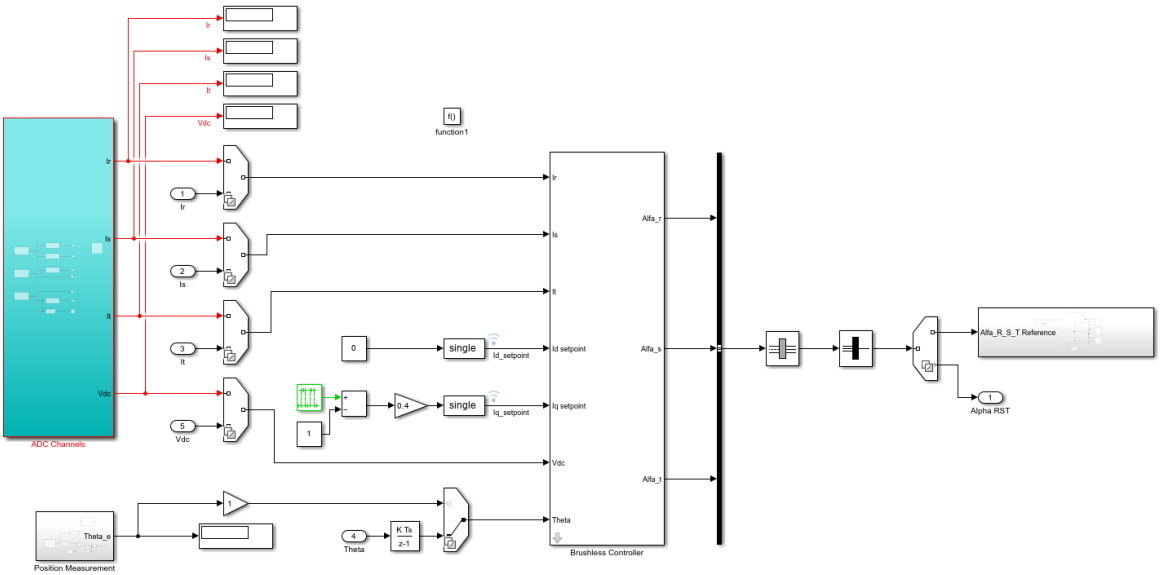

Fig. 14 - ADC Interrupt, Controller second layer

4.1.2.2. ADC Channels

The ADC blocks perform analog-to-digital conversions of the signals connected to the selected ADC input pins. The ADC block outputs digital values representing the analog input signal and stores the converted values in the resulting register of the digital signal processor [11]. For this particular implementation, block C2802x/03x/05x/06x is used. The ADC outputs a constant stream of data collected from the ADC pins on the DSP.

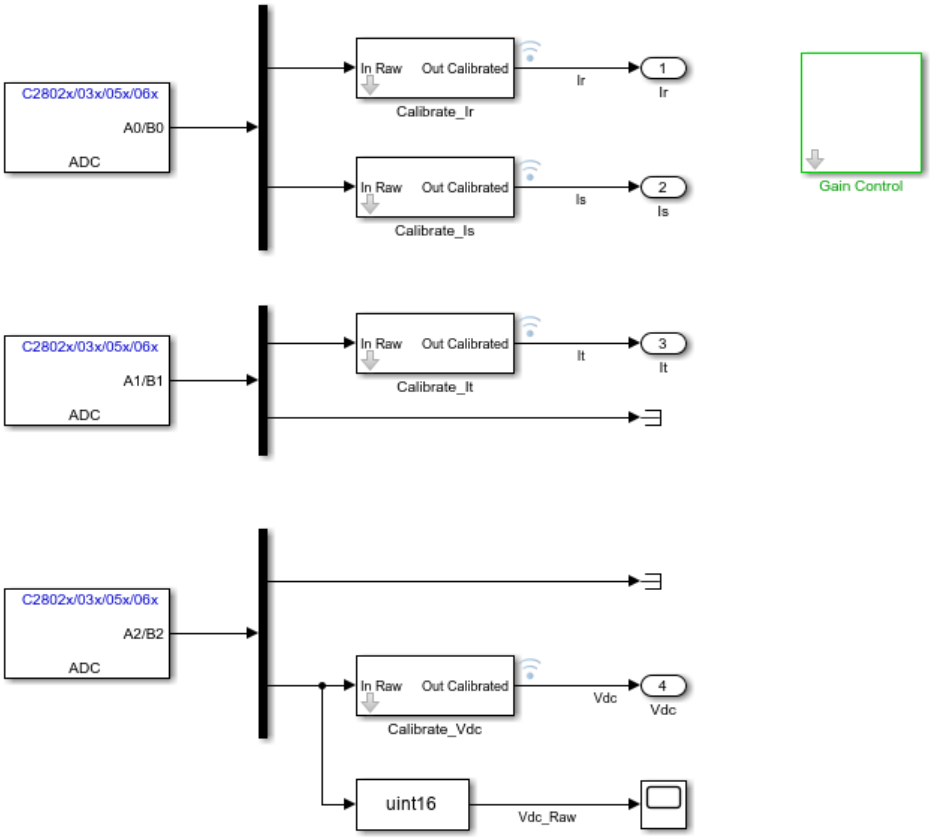

Fig. 15 – ADC Channels subsystem, signal calibration

If the block is configured to perform samples simultaneously, two SOC can be selected and it samples the corresponding channels of modules 1 and 2 at the same time. Hardware allows each signal of a pair to be sampled simultaneously. The ADCs blocks shown in figure 15 are executed sequentially and each block processes to samples (two outputs).

For this application, the first two ADC will sample the currents, while third it is sampling the voltage. The last ADC also post interrupt at the End of Conversion (EOC), which indicates the interrupt that the ADCs have finished processing the signals, as indicated in the figure 17.

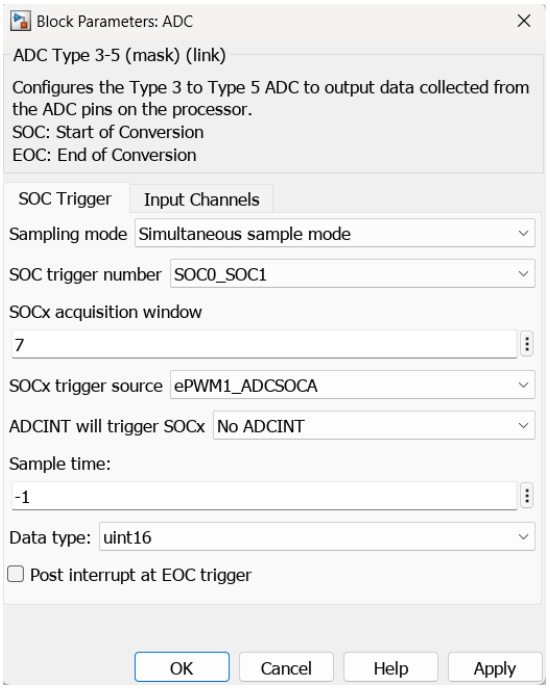

Fig. 16 – Current reader ADC blocks parameters

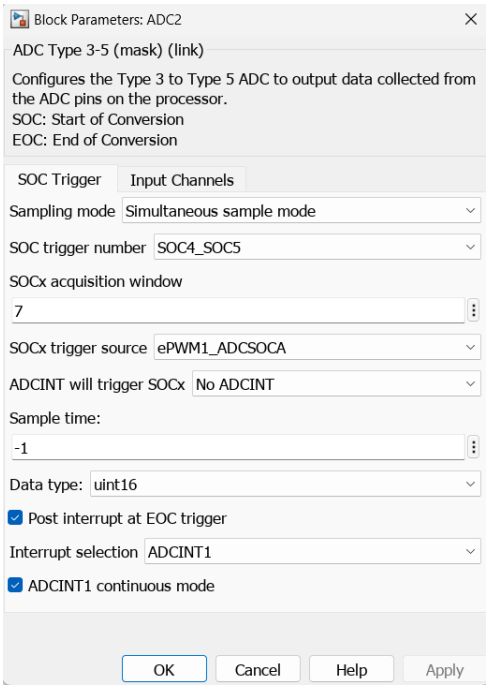

Fig. 17 – Voltage reader ADC block parameters

The output signal from the ADC requires additional calibration to be used in the control algorithm. It is measured from the low-side current shunt sense for each half-bridge (phases *r*, *s*, and *t*). As the inverter manufacturer comments: "*The differential amplifier senses voltage across a 0,007 Ω power sense resistor with differential connections. The differential voltage is then amplified by 10 V/V and centered at 1,65 V to allow for sensing of both positive and negative currents. The sense resistor has been scaled for 0 A to 20 A peak currents.*" [12]

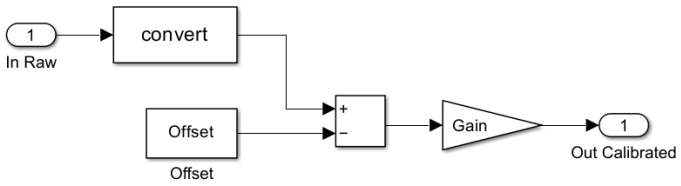

Fig. 18 – Current calibration subsystem

Therefore, the offset is half the ADC resolution because the voltage is centered, and the gain to convert the read signal into the actual current in the pin is as follows. Both operations were performed by using a mask for the calibration block.

$$Offset = \frac{2^{12}}{2} - 1 = 2047$$

$$Gian = \frac{1{,}65}{2047 \cdot 0{,}07 \cdot 80}$$

Mention that the output of this subsystem is of relative importance since it is the reading of the parameters that will later be used for the closed-loop control. In case of not configuring the output correctly or miscalibrating the signal, the control system could damage some components.

4.1.2.3. Voltage Gain Calibration

As mentioned in the previous section, the differential voltage is amplified to 10 V/V by default. However, this reading may still be very small because a low voltage is being used. To eliminate possible problems, a complementary subsystem has been assembled that allows the inverter gain to be modified. In this way, more current can pass through the bus through the Serial Peripheral Interface (SPI).

In the mask of the block, a new Gain per phase can be specified. For example, with a gain of 40 V/V, four times the intensity is sent. The subsystem detects whether a change has been introduced into the configuration and sends a new gain to the system.

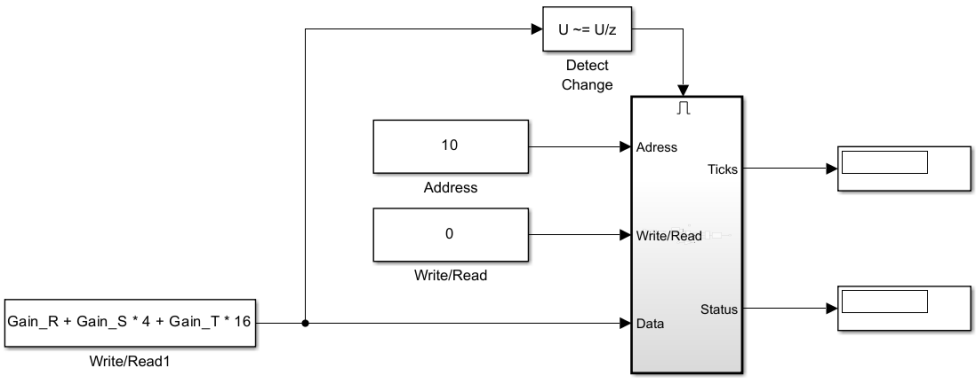

Fig. 19 – Current calibration subsystem

4.1.2.4. Position Measurement

To correctly implement the motor control using SVPWM, it is necessary to know the angle of the rotor. In this case, encoder reading is used to obtain the position and, therefore, the angle.

The enhanced quadrature encoder pulse (eQEP) block is used along with an encoder to obtain the position from a rotating machine. It is set to output the encoder counter, which has 4000 counts/rev (post-quad) resolution and an index pulse repeatability of ± 1 count for resolutions ≥ 4,000 counts/rev. Moreover, the motor has four pole pairs; therefore, in order to obtain the correct angle for the calculations the obtained angle from the eQEP must be multiplied by four.

Figure 20 shows the position-measurement subsystem with the aforementioned transformations. Note that there is an optional block to add an offset to the angles, although it was not necessary.

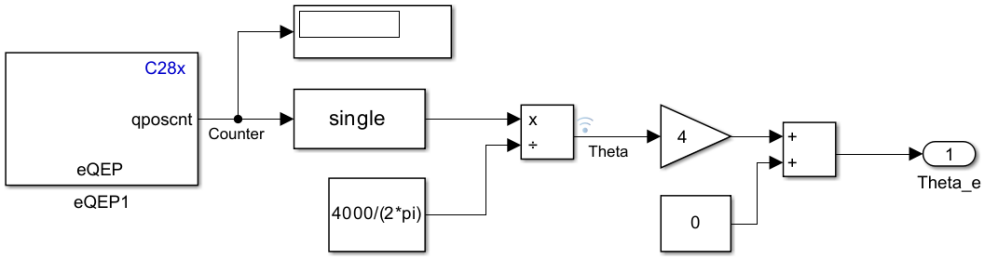

Fig. 20 – Position measurement subsystem

4.1.2.5. Brushless Controller

The control system is a closed-loop control system based on the concepts previously mentioned in the project report. Clake and Park transformations were performed to obtain the intensity in reference to the *d* and *q* axes from the signals provided by the ADCs. The operation of each block is not discussed in detail because there are different libraries and addons that allow these transformations to be carried out.

Subsequently, the obtained signal is compared with the setpoint currents using a PID, resulting in a rectified *dq* value. Another step is required to set the PID *dq* calculated values in the reference of the fixed stator axes. For this purpose, the Inverse Park transformation is used, which requires the mechanical angle to determine how to transform the *dq* rectified currents to the *alpha-beta* reference axes.

Finally, the alphas were obtained using the SVPWM method. As mentioned in the 3.3. Space Vector Pulse Width Modulation section, the *dq0 (*or *alpha-beta)* currents cannot go back to the *abc* reference thus SVPWM is used. This calculation can be performed in several ways. In this case, a library is used that executes a MATLAB script in which the corresponding matrix is applied according to the sector in which vector *q* of the motor is found.

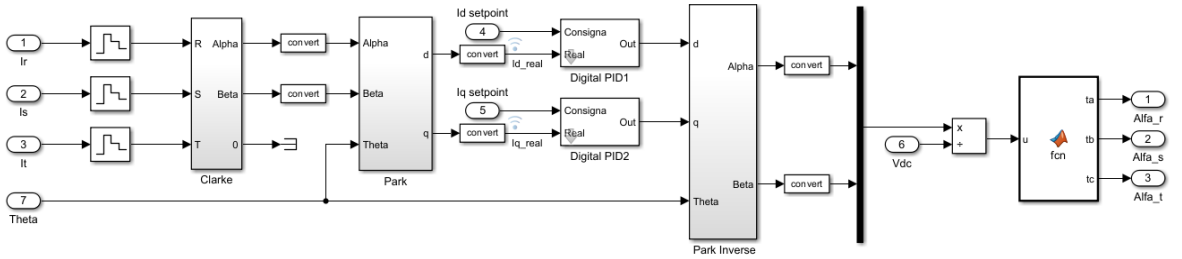

Fig. 21 – Brushless Controller subsystem

Outside the Brushless Controller subsystem, if the system is being simulated, the alphas will come out of the controller to be sent to the plant. Otherwise, if the code is being generated, the alphas are sent to the inverter to generate PWM signals. It has been decided to include this subsystem within the controller to simplify the final code by depending only on the module (feedback_controller.slx). This configuration is described in detail in the following section.

4.1.2.6. Three Phase Inverter

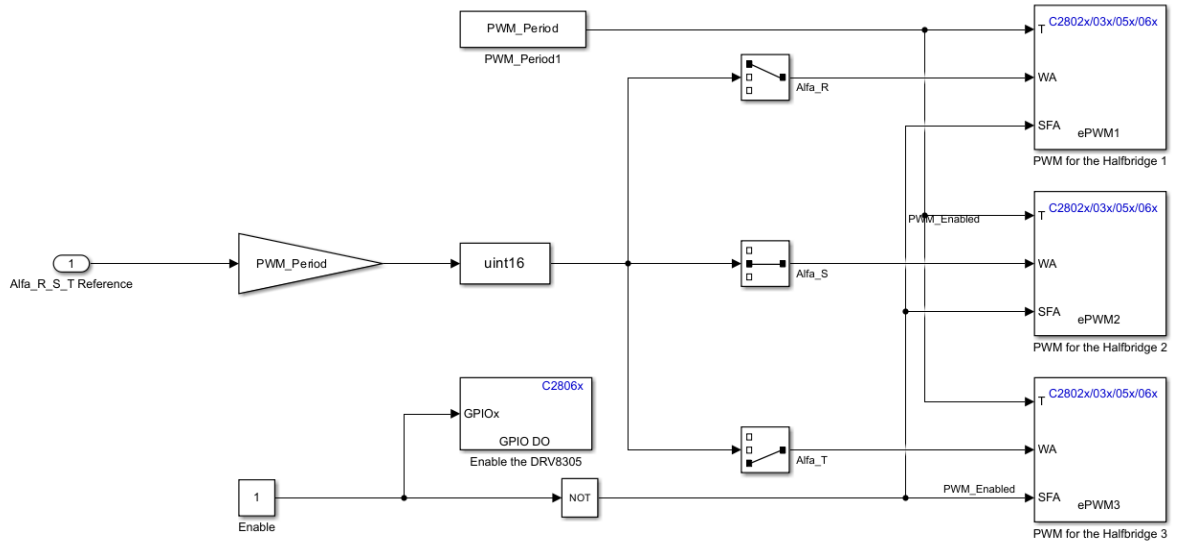

Fig. 22 – Controller three phase inverter, PWM signal generator

Multiple ePWM modules are available on the C28x devices to generate PWM waveforms. In this implementation, the C2802x/03x/05x/06x block is used. Each module generates two PWM signals ePWMA and ePWMB, although in this case only the ePWMA is taken into account. [13]

The first ePWM (ePWM1) serves to synchronize the other blocks, although their general configurations are very similar. The configuration used for ePWM1 is described in detail using captures below. The necessary changes for ePWM2 and ePWM3 have been explained with comments. Thus, the entire inverter configuration is presented visually to replicate the test. The configuration options that were not mentioned were set as default.

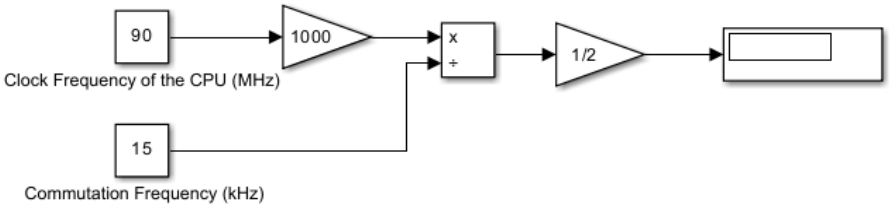

Fig. 23 – Controller three phase inverter, PWM signal generator

Each block receives its corresponding alpha multiplied by the commutation period, commutation period itself (PWM_Period), and an enable signal. This signal serves as a protection measure and allows the operation of the inverter to be stopped and, therefore, the entire system. Meanwhile, the desired commutation period can be obtained by dividing the clock frequency by twice the commutation frequency, as shown in figure 23.

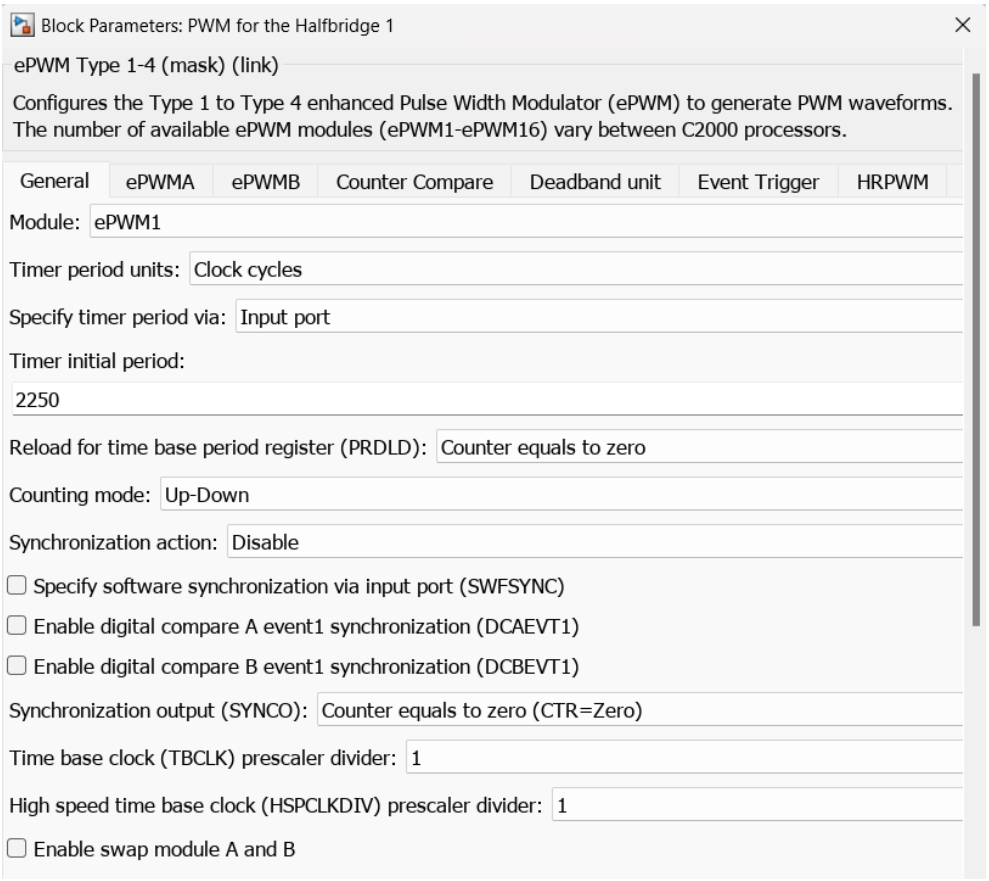

Fig. 24 – ePWM1 General configuration

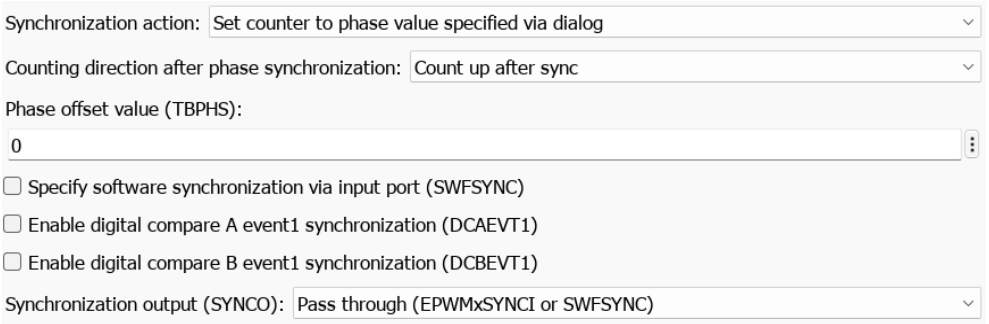

Fig. 25 – ePWM2/3 General configuration

Therefore, the timer period and the CMPA (Fig.27) are set to be specified from outside the block via an input port. On the one hand, for ePWM1, the synchronization action is disabled and the output (SYNCO) is set to counter equal to zero. On the other blocks, the synchronization action is to set

counter to the phase value counting up, and SYNCO is set to pass through; thus, the ePWM1 synchronization signal is not disrupted.

Next, the PWM signal must be enabled and the actions to be taken according to the CMPA received configuration. The following figure shows the configuration used for all the ePWM blocks.

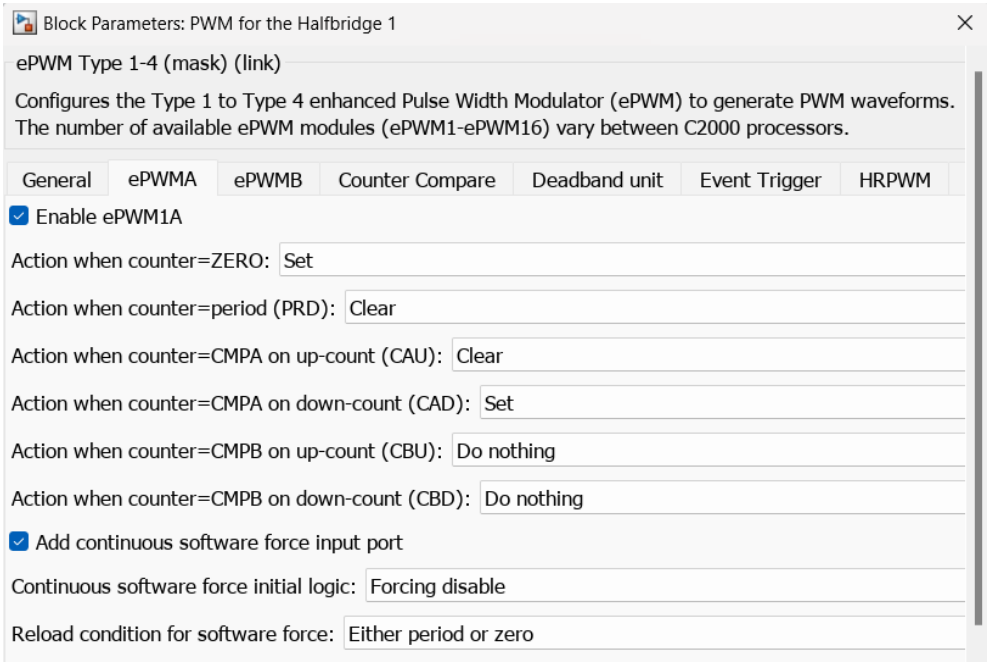

Fig. 26 – ePWM1 - ePWMA signal

Because only the ePWMA signal is used, only Comparer A needs to be specified. As seen in figure 26, Compare A Register reload when the counter is equal to zero or period. This configuration is the same for all blocks.

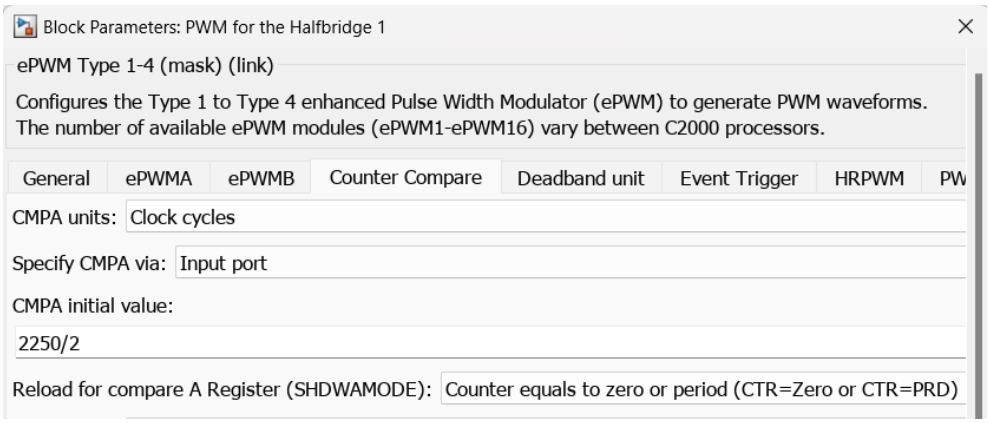

Fig. 27 – ePWM1 Counter Compare

For the Deadband unit configuration, ePWMA is the signal source for both the raising and falling edges with a deadband period of 30 clock cycles. This enables a deadband area of the rising-edge delay and falling-edge delay cycles without signal overlap between pairs of ePWM output signals.

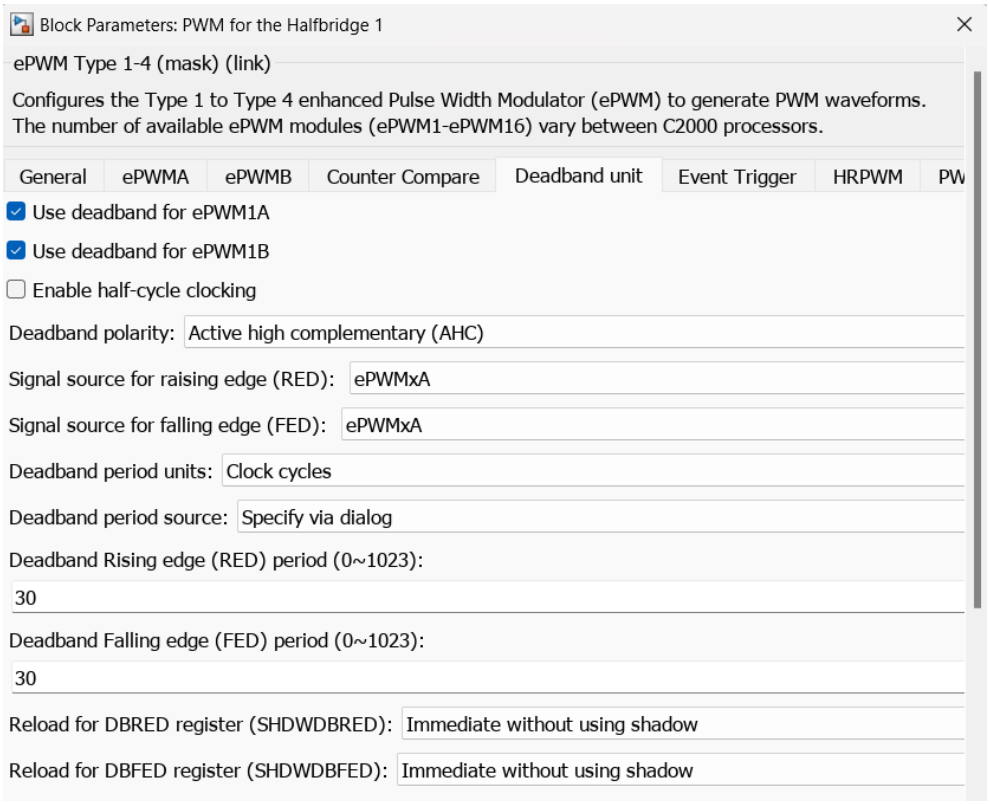

Fig. 28 – ePWM1 Deadband unit

Finally, ePWM1 also triggers the ADC start of the conversion for model A (SOCA). First event triggers the ADC start of conversion with every event when the indicated countermatch condition; in this case, when the counter is equal to period. This configuration is exclusive to this ePWM because it is only necessary to be send it once.

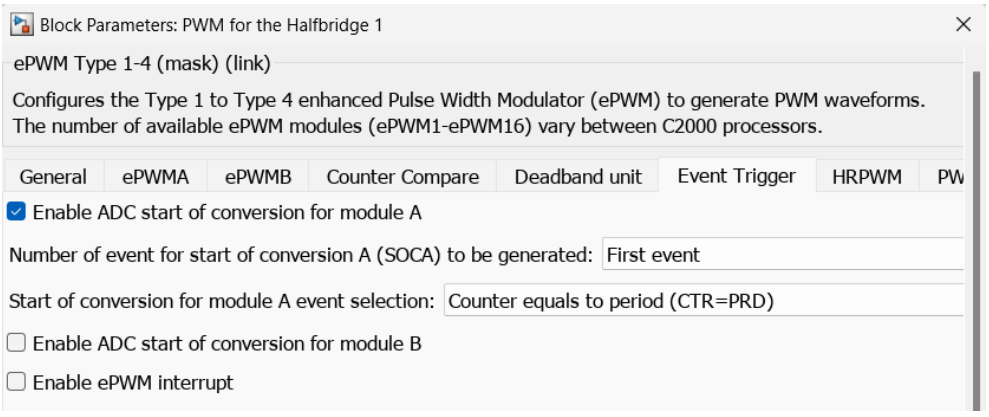

Fig. 30 – ePWM1 Event Trigger

4.1.3. Plant

As previously mentioned, the plant is active only if the system is simulated and receives the alphas calculated in the controller. In addition, the voltage must be specified; in this case, 20 V, which simulates the voltage source. On the other hand, by means of a transfer function, the angle of rotation is obtained from the torque of the motor. The coefficients used were $\frac{1}{j \cdot s + b}$, where *j* is the motor inertia and $\frac{1}{b}$ is the gain in the continuous voltage. Some simplifications have been made, such as dry scrubbing being proportional to the speed and b being equal to the scrubbing losses (approx. 2%).

This information is necessary to correctly apply Park as well as the intensity in the after phases. Therefore, the angle is sent to the controller through an output of 4.

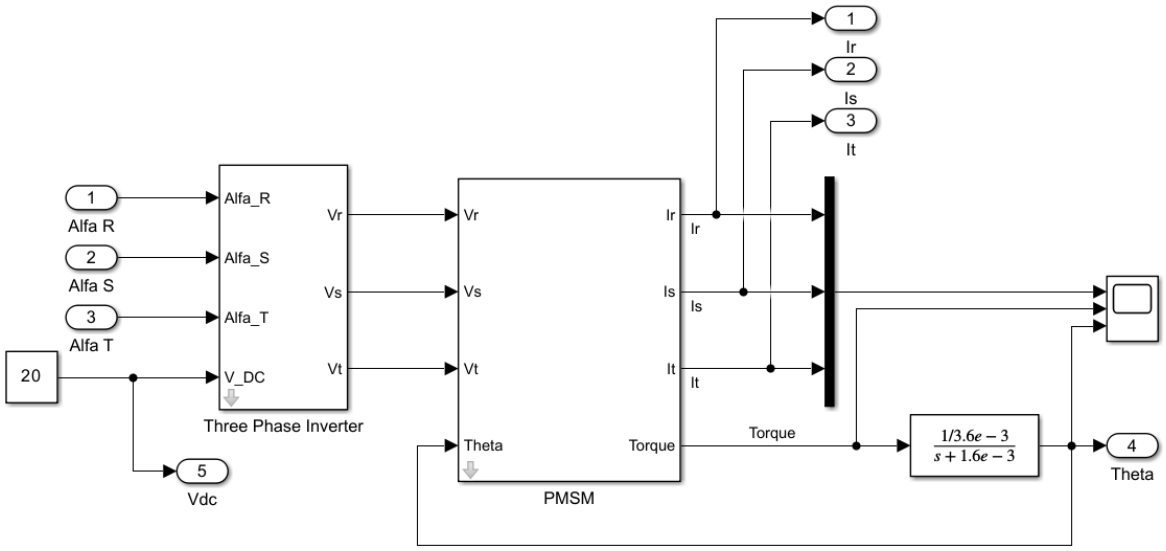

Fig. 31 – Plant model

There are two subsystems in the plant that simulate the physical components of the system: the three-phase inverter and PSMS motor. Note that the models used in the simulation are simplifications of the physical system used for computing power. Even with these simplifications, the plant should simulate the physical system precisely and obtain similar results.

4.1.3.1. Three Phase Inverter

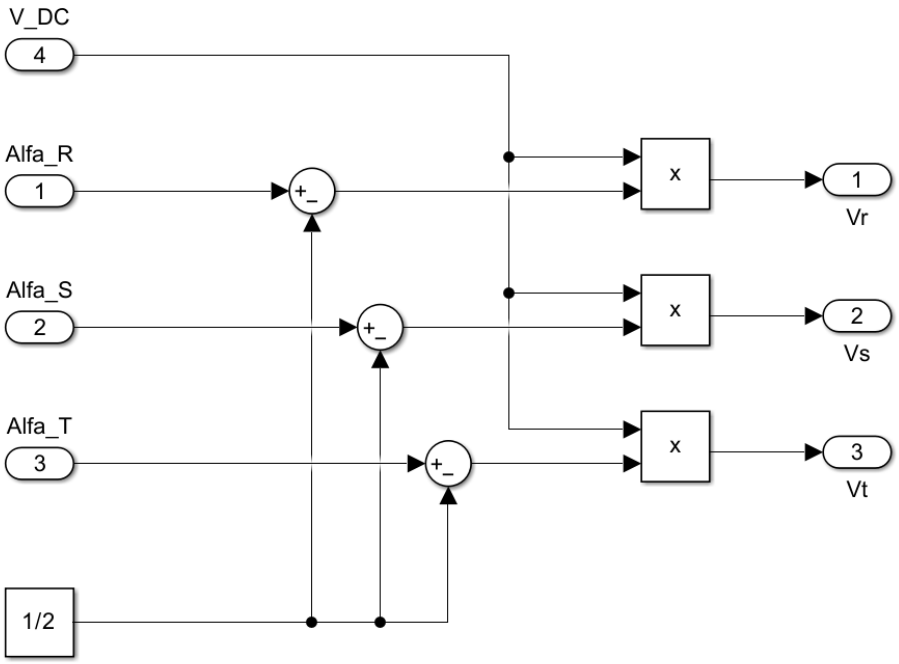

Fig. 32 – Simplified three phase inverter model

An averaged model was used for the inverter because of its simplicity and ease to calculate. This model receives the alphas calculated by the controller and voltage from the power source, which is located inside the plant model. Then, 0,5 is subtracted from the alpha of each phase and multiplied by the voltage.

Thus, a constant voltage is applied throughout the period equivalent to the average voltage that would be applied during the operating time of the alphas. This simplification eliminates the ripple that appears in the voltage when the alphas are applied correctly. However, the overall response of the system is not affected.

4.1.3.2. Permanent Magnet Synchronous Motor

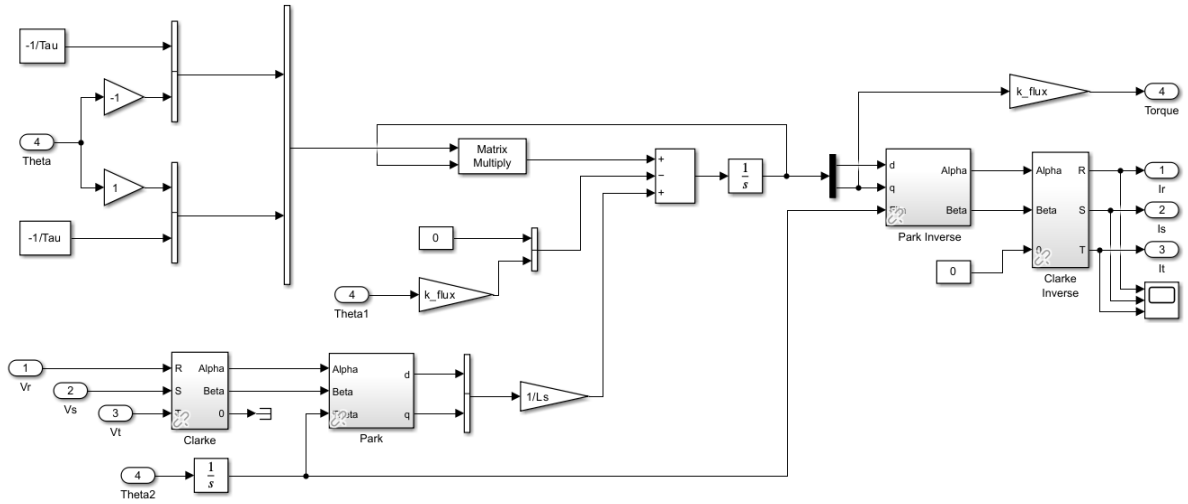

Fig. 33 – PMSM model

Some of the principles used in the controller have also been applied to the motor model. First, it is based on differential equations that describe the behavior of a brushless motor.

$$\begin{bmatrix} v_r \\ v_s \\ v_t \end{bmatrix} = \begin{bmatrix} R_s & 0 & 0 \\ 0 & R_s & 0 \\ 0 & 0 & R_s \end{bmatrix} \cdot \begin{bmatrix} i_r \\ i_s \\ i_t \end{bmatrix} + \frac{d}{dt} \left(\begin{bmatrix} L_{sd} + M & -\frac{1}{2}M & -\frac{1}{2}M \\ -\frac{1}{2}M & L_{sd} + M & -\frac{1}{2}M \\ -\frac{1}{2}M & -\frac{1}{2}M & L_{sd} + M \end{bmatrix} \cdot \begin{bmatrix} i_r \\ i_s \\ i_t \end{bmatrix} + \begin{bmatrix} \psi \cdot \cos(\alpha) \\ \psi \cdot \cos\left(\alpha + \frac{2\pi}{3}\right) \\ \psi \cdot \cos\left(\alpha - \frac{2\pi}{3}\right) \end{bmatrix} \right)$$

Subsequently, by applying Park and Clark transformations to the voltage, an equivalent system of equations referenced on the *dq* axes can be obtained. These calculations were taken from Joan Bergas's thesis [10], and it has been decided to explain them step-by-step in Annex 1 because it is not the main topic of this thesis.

$$\begin{bmatrix} V_d \\ V_q \end{bmatrix} = \begin{bmatrix} R_s & -w \cdot L_s \\ w \cdot L_s & R_s \end{bmatrix} \begin{bmatrix} I_d \\ I_q \end{bmatrix} + \begin{bmatrix} L_s & 0 \\ 0 & L_s \end{bmatrix} \frac{d}{dt} \begin{bmatrix} I_d \\ I_q \end{bmatrix} + \begin{bmatrix} 0 \\ \sqrt{\frac{3}{2}}\, w_m\, \psi \end{bmatrix}$$

In addition, to determine the torque of the brushless motor, the expression obtained from electromechanical conversion can be applied.

$$\Gamma(t) = \frac{1}{2}[i]^t \frac{d}{d\alpha}[M(\alpha)][i]$$

It is assumed that in the roto there is a field created by an inductance and, once operated, the torque expression remains as follows:

$$\Gamma(t) = M \cdot i_{iman} \left(-i_r \cdot \sin(\alpha) - i_s \cdot \sin\left(\alpha - \frac{2\pi}{3}\right) - i_t \cdot \sin\left(\alpha + \frac{2\pi}{3}\right) \right)$$

This expression can be easily verified to be equivalent to:

$$\Gamma(t) = \varphi \cdot I_q$$

Therefore, the torque can be easily obtained by referring to the *dq* axes. By performing these transformations, the model is simplified, allowing the simulation time to be reduced, and iterations of the system could be performed. Otherwise, it would have to work with a system of three equations with nonconstant coefficients.

Finally, the process and transformations mentioned in Annex 1 were applied to Simulink to build the motor simulation model. In contrast to the inverter, even though it is a model that simplifies the calculations, it should accurately represent the real motor.

4.2. Implementation

The implementation of the control was carried out in three phases: the first where the signals generated by the controller and inverter were checked manually, the second where the connectivity was tested with the entire system assembled, and the third in which the parameters were modified in real time.

In the first test, the output signals generated by the inverter have been analyzed, as well as other signals, such as the position reading and the alphas calculated by the controller. This control test was carried out in an open loop with the minimum voltage to avoid damage to any component. An oscilloscope was used to monitor the various signals. This step is important to verify that the controller generates the correct signals at the specified output ports. This would be a problem when controlling the system in a closed loop and reading wrong inputs.

Furthermore, auxiliary blocks and subsystems were used for the checks, which were subsequently eliminated in the final control code. Using the ePWM block, it is possible to send a signal to its output pin to be read from an external source, such as an oscilloscope. For example, by using ePWM8, which is connected to GPIO42 with output pin 72, it is possible to read the I_q setpoint. Additional signal calibration is required to synchronize the signal with the clock frequency of the processor.

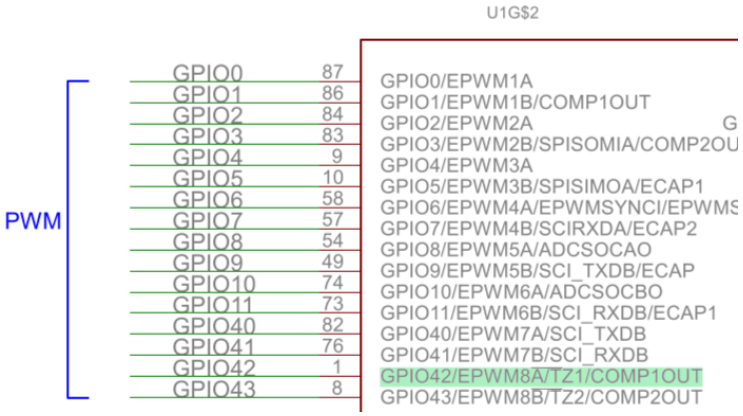

Fig. 34 - LAUNCHXL-F28069M PWM - GPIO connections

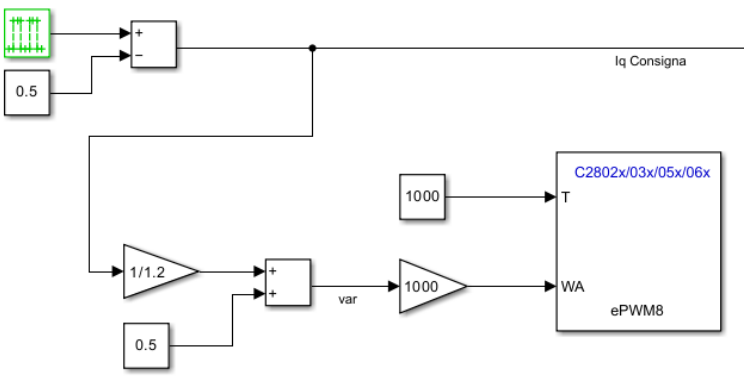

Fig. 35 - Auxiliary output subsystems example

In the second test, the complete system was assembled and its connectivity was verified. Similarly, the minimum voltage was used to turn the motor. The objective was to check the reading of the motor information and the response of the system in real-time. To do so, in an external mode simulation, a serial XCP communication channel was used. This communication protocol allows the tuning of parameters in real time and monitors target application signals.

In this case, during the simulation, some signals were monitored using a Scope block, and parameters were tuned using Dashboard blocks or by modifying the value of the block directly. This algorithm requires additional configuration, as the Storage Class for desired variables needs to be set as Exported Global. This is easily configurable through the Embedded Coder > Code Mappings - Component Interface > Signals. Then, a flag icon must appear next to the variable, as shown below.

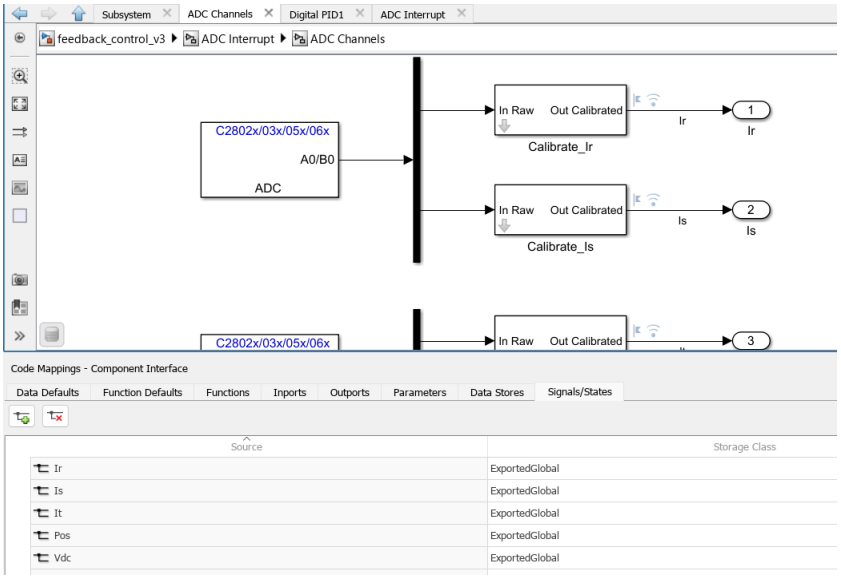

Fig. 36 - Signal logged to be ExportedGlobal

Finally, the response of the system to changes in the parameters in real time was tested. In addition, the profiles for the setpoint signals were preset and verified with the real performance of the system.

On the other hand, loads are established on the motor with the intention that the system will correct its behavior. All the experiments are detailed and documented in section 4.2. Experimental results.

4.2.1. Hardware

In this section the hardware used in the implementation of the control algorithm is mentioned.

- **AC motor**: The motor being controlled is the main component of the experiment. Specifically, the Industrial-Grade NEMA 23 Motor from Teknic [14] has been used. As mentioned earlier, it is a permanent magnet synchronous motor (PMSM) with the following characteristics:
    - Model: 2310
    - Electrical Interface Option: P
    - Resistance, phase to phase: 0,72 Ω
    - Inductance, phase to phase: 0,4 mH
    - Electrical Time Constant: 0,56 ms
    - Back EMF (Ke): 4,64 V peak/kRPM
    - Continuous Torque: 39 oz-in

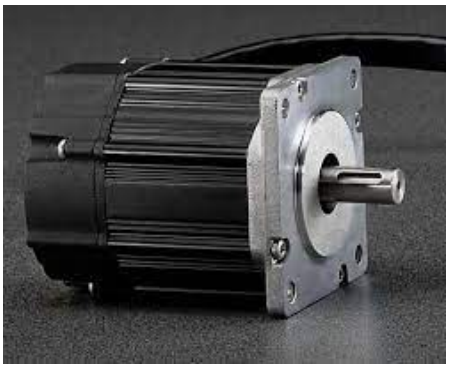

Fig. 37 - IndustrialGrade NEMA 23 Motor

It has 8 poles and it uses fully sintered, high temperature, Neodymium-Iron-Boron magnets with an optimized stator design. Moreover, it incorporates a floating optical disk single-ended encoder with 4000 counts/rev (post-quad) resolution and an index pulse repeatability of ± 1 count for resolutions ≥ 4,000 counts/rev.

- **Microcontroller**: It is used to generate the control signals for the inverter. This test is performed on a *C2000™ Piccolo™ LaunchPad™, LAUNCHXL-F28069M*. According to the manufacturer: "*It is a complete low-cost development board for the Texas Instruments Piccolo F2806x devices and InstaSPIN technology. The LAUNCHXL-F28069M kit features all the hardware and software necessary to develop applications based on the F2806x microprocessor. It is based on the superset F28069M device. It offers an on-board JTAG emulation tool allowing direct interface to a PC for easy programming, debugging, and evaluation. In addition, the USB interface provides a universal asynchronous receiver/transmitter (UART) serial connection from the F2806x device to the host PC.*" [15]

This decision has been made mainly due to the thesis director's knowledge of the board and the great documentation available. Also, it's a relatively simple development kit with enough ports for this project.

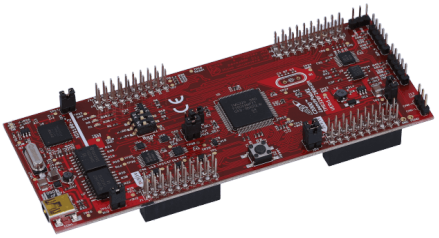

Fig. 38 - LAUNCHXL-F28069M board

- **Three-phase inverter:** A three-phase inverter is used to convert DC power into three-phase AC power. It consists of six switches that can be controlled to produce a sinusoidal output voltage waveform with adjustable amplitude and frequency. In combination with the *LAUNCHXL-F28069M*, for this experiment the *BOOSTXL-DRV8305EV BoosterPack* is going to be used. "*It is a complete 3-phase driver stage in order to evaluate motor application with the DRV8305 motor gate driver. It utilizes a compact and modular form factor for ease of use and is designed to dock with compatible TI LaunchPad™ development kits for a complete motor control system.*" [12]

- **Power supply**: A DC power supply is required to power the inverter and, in consequence, the motor. For this particular project, a standard 12-24 V source is enough, since we will control the current that the motor receives with the inverter. The lower the voltage, the slower the motor will move but it should not affect the general operation of the system. Tests have been made with a minimum voltage of 7 V. The model used is AX-3003D from AXIOMET, capable of delivering 0-30 VDC / 0-3 A.

- **Oscilloscope**: An oscilloscope is used to measure the output voltage waveform and to observe the effect of the control algorithm on the motor performance. Although not strictly necessary, it is a way of physically measuring signals. On the other hand, since the closed-loop control is carried out, the parameters to be controlled are known and can be displayed through Simulink. PicoScope 2000 Series oscilloscope was used during the testing phase.

- **Cables and connectors**: Additionally to the motor/encoder cables, more cables are needed to connect the power supply and inverter.

Moreover, safety precautions should always be taken when working with high voltage and electrical equipment. The experiment has been carried out in a controlled laboratory with constant supervision.

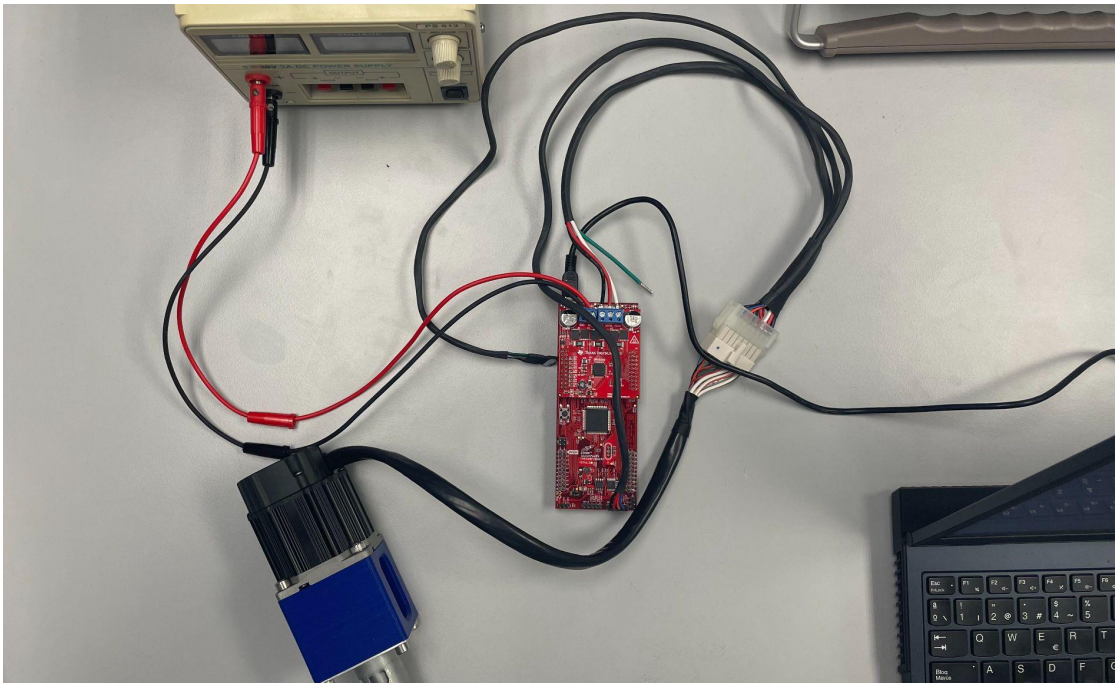

Fig. 39 - LAUNCHXL-F28069M board

Figure 39 shows the assembled physical system. First, the inverter is mounted on top of the controller and the voltage sources and the three phases of the motor are connected to it. The motor encoder output was connected to its corresponding pins at the lower part of the controller. Finally, the controller was connected to the laptop through the micro USB port.

4.3. Experimentation and Testing

4.3.1. Simulation model results

Tests were conducted with different loads to verify the response of the simulation model. These are very simple tests with the intention of being replicated in the physical system and comparing the responses of the system. Note that the setpoint variables are I_d and I_q , although I_d is always zero.

To visualize the response, the I_{rst} current, torque, *theta* (representing the movement of the motor), and setpoint signals are displayed in the same scope. The first test was used to calibrate the control parameters, particularly the motor position readings. For this reason, a constant value I_q command was set.

Figure 38 shows the correct operation of the motor. It can be observed that the voltage becomes saturated, reaching the maximum speed that the bus allows. Meanwhile, the torque was approximately 5 Nm. As mentioned above, torque is proportional to I_q, and coincidentally, in this case, k_{flux} is almost 1 Nm/A.

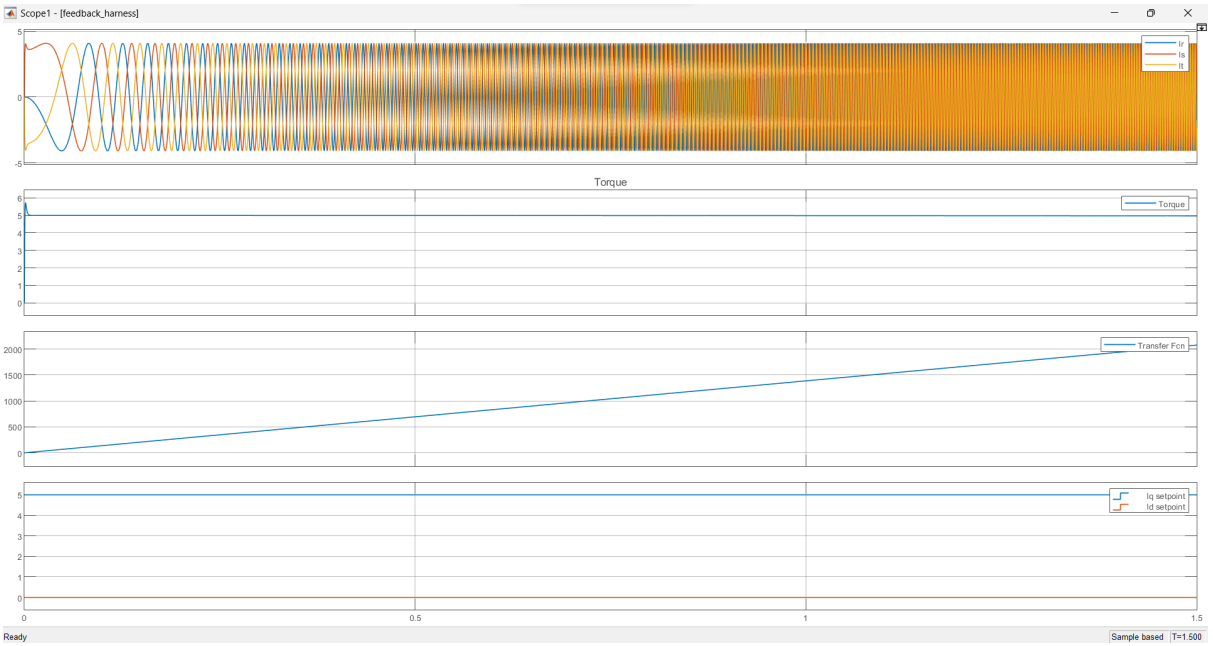

Fig. 40 - Simulation model Test 1: I_r I_s I_t [A], Torque [Nm], *Theta* [rad], Setpoint I_d I_q [A]

In the second test, a step setpoint I_q was set from 10 A to -10 A. This makes it possible to observe the response of the system to changes in the direction of rotation of the motor, in addition to verifying that it can admit setpoint currents with a negative value.

Figure 41 shows an enlargement of the area where the step acts. In this case, a current peak is observed, although this does not invert its order. The direction of rotation of the motor has now changed and the angle of rotation value starts to decrease.

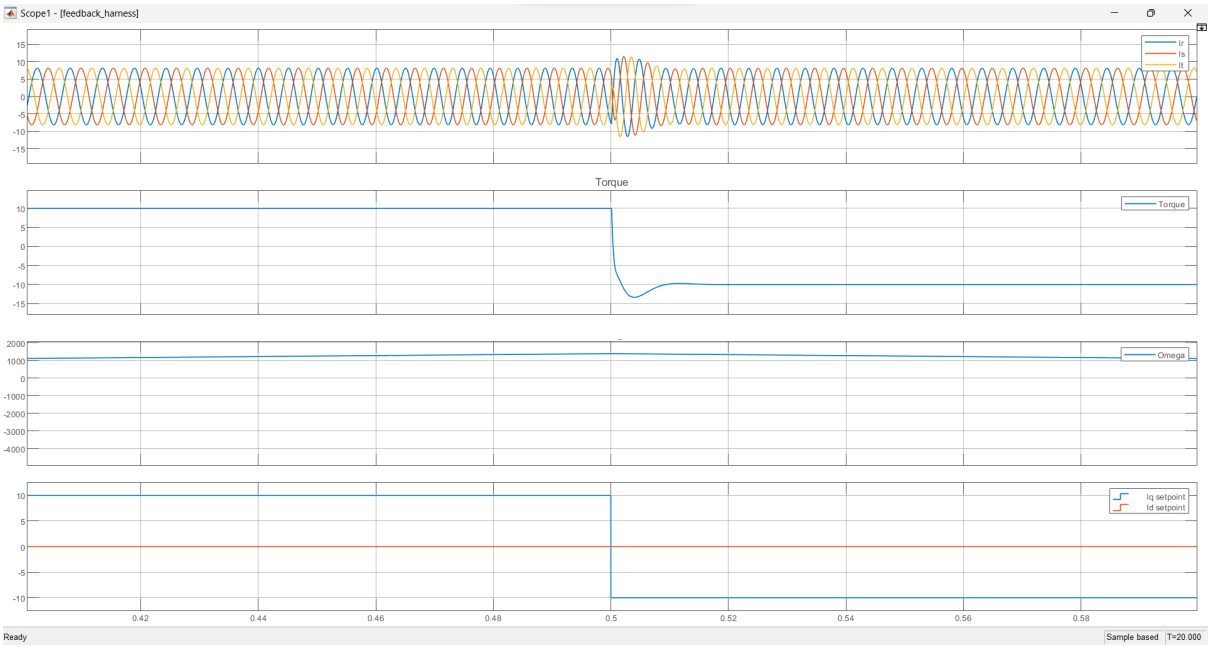

Fig. 41 - Simulation model Test 2 detail (0,4 - 0,6 s): I_r I_s I_t [A], Torque [Nm], *Theta* [rad], Setpoint I_d I_q [A]

Figure 42 shows how the angle of the motor continues to decrease until it acquires a negative value. At this point, the current reverses its order from the *rst* to *tsr* phases. However, the motor does not change its direction of rotation.

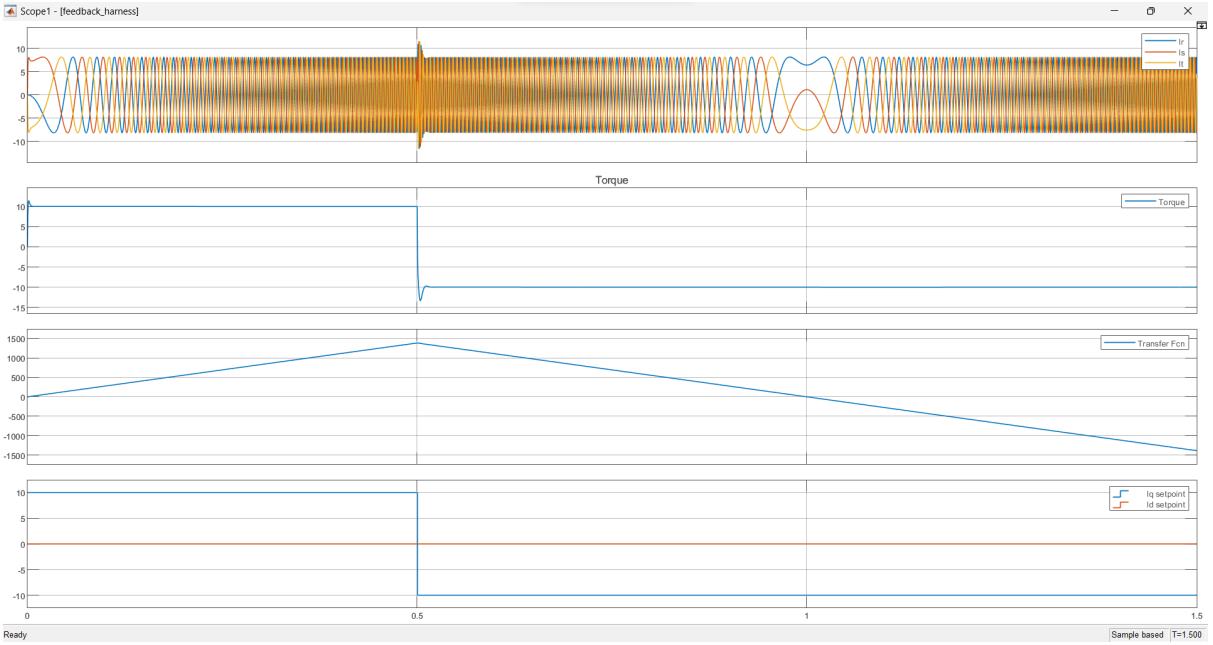

Fig. 42 - Simulation model Test 2: I_r I_s I_t [A], Torque [Nm], *Theta* [rad], Setpoint I_d I_q [A]

Finally, the last test consisted of giving it a cyclic setpoint I_q with an action time of 0,1 s and a load value of 5 A. Both in the position and in the torque, the motor activity can be observed.

Regarding the currents, a behavior similar to the first test can be observed, where it gradually saturates, although with a greater delay because there are moments of inactivity. In addition, when turning the motor again, a current peak is produced in the first phase. Figure 44 shows the details of the complete cycle.

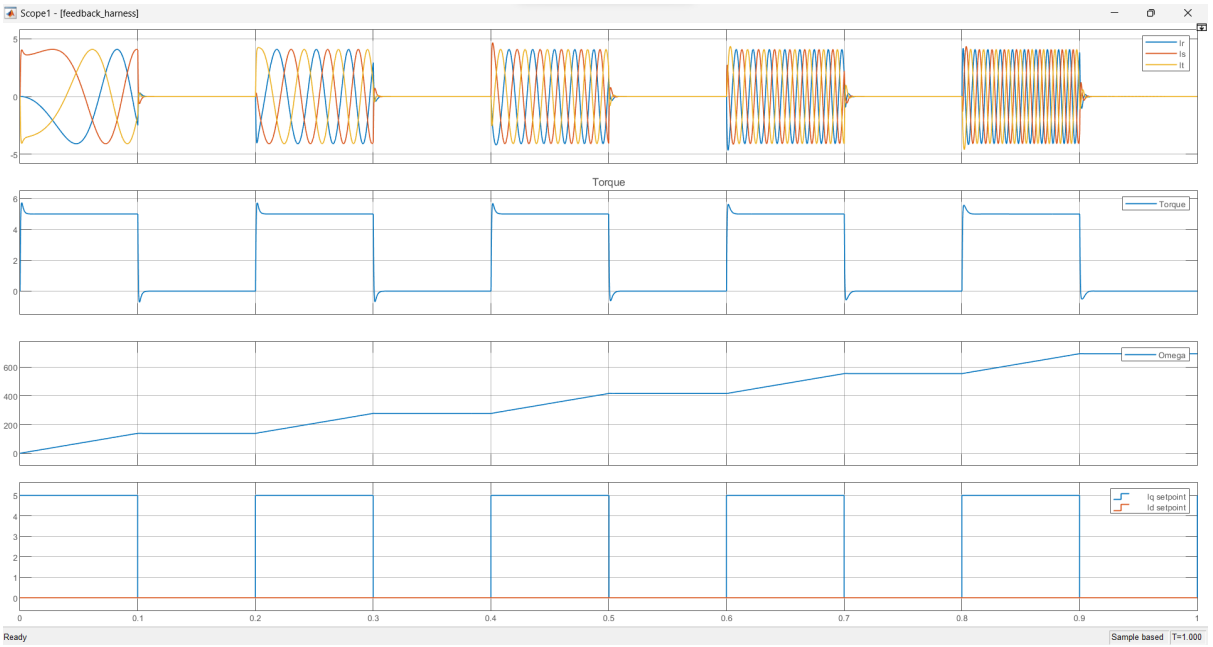

Fig. 43 - Simulation model Test 3: I_r I_s I_t [A], Torque [Nm], *Theta* [rad], Setpoint I_d I_q [A]

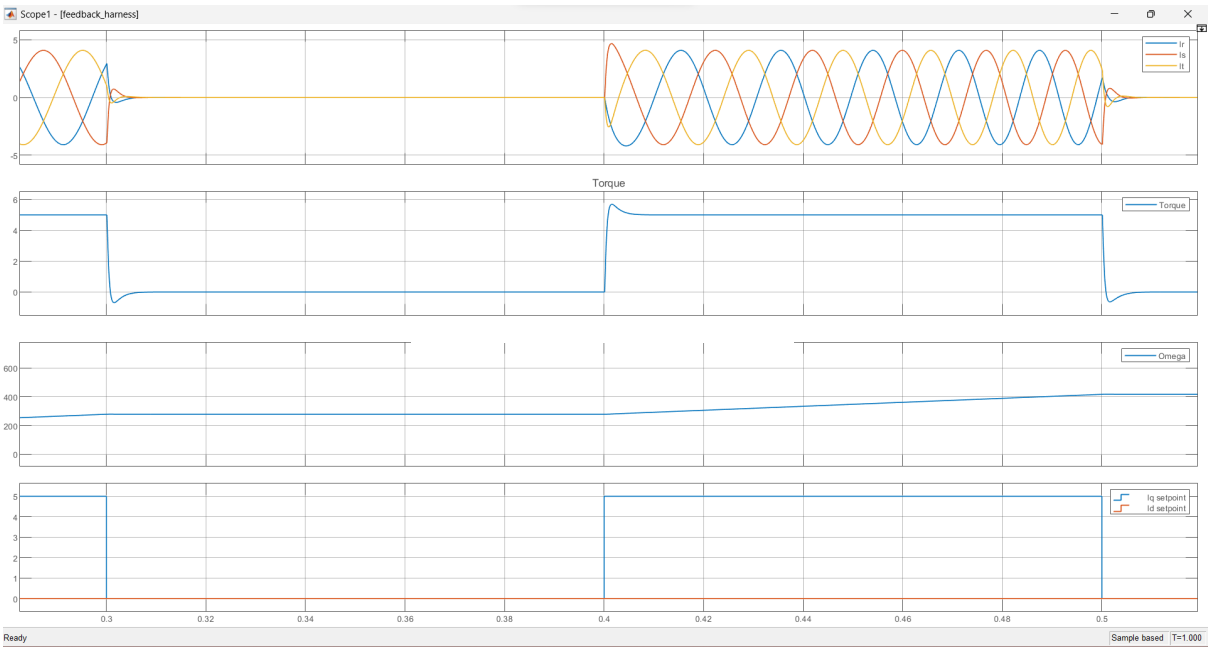

Fig. 44 - Simulation model Test 3 detail (0,3 - 0,5 s): I_r I_s I_t [A], Torque [Nm], *Theta* [rad], Setpoint I_d I_q [A]

4.3.2. Experimental results

Mention that all results were obtained directly from the launchpad and, because the serial communication between the target hardware and laptop is limited to less than 6 Mbps, the signals obtained present considerable noise and poor resolution.

This problem could have been solved by repeating the same test several times and visualizing only one signal to increase the information sent or capturing the signals with an external oscilloscope. Even so, because the behavior of the system can be observed, it was decided to group the signals in fewer captures and not lengthen the memory of the project unnecessarily.

To adjust the control parameters, the first test has also been a low-value constant I_q (0,4 A). In this case, the scope displays the angle, which represents the movement, the current of the three phases, and a comparison between the setpoint I_q and the real one. When completing a turn, the encoder resets and marks 0; therefore, the angle obtained will always be between ±4000 and 0, or its equivalent in radians $\pm 2\pi$ rad and 0 rad.

Figure 45 shows how the I_q current and phase currents remained stable with little noise. However, the signal of the angle could have aliasing, which is that its sampling frequency is slower than the real frequency of the angle. Ignoring this factor, the behavior of the angle is also expected.

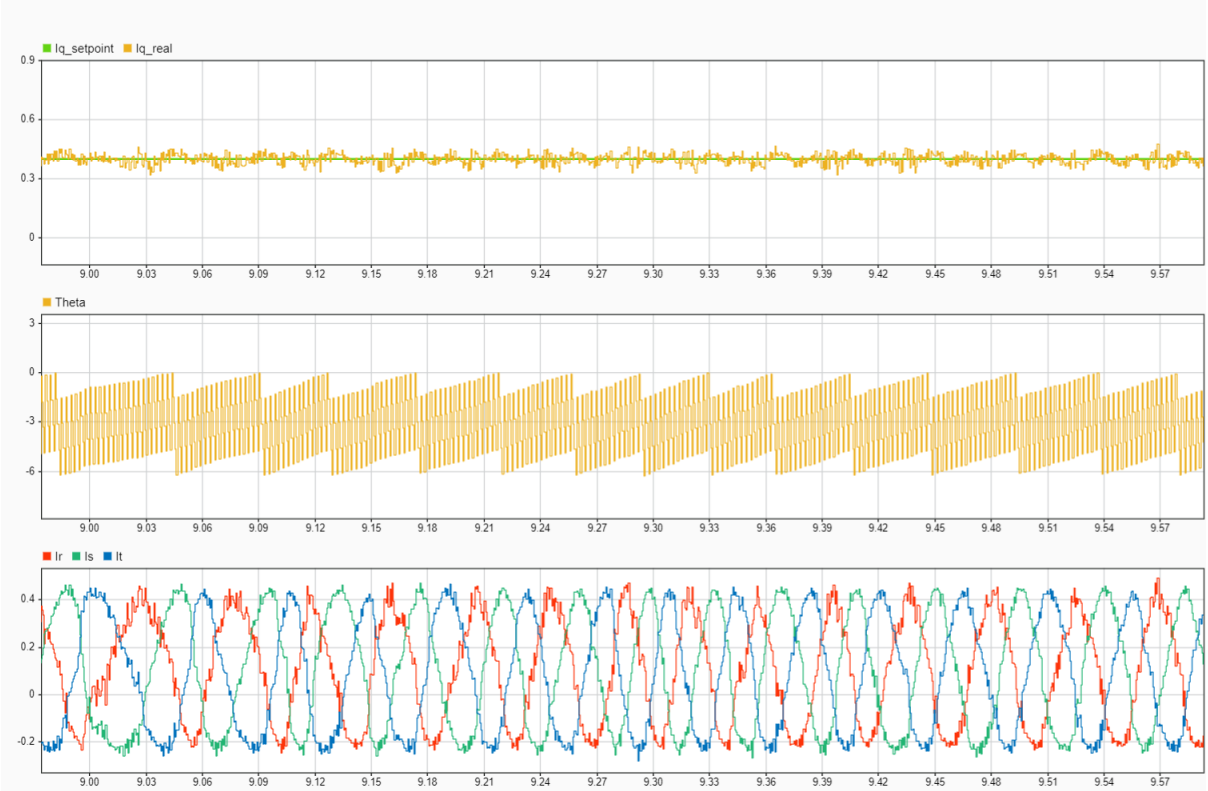

Fig. 45 - Experimental Test 1: Setpoint I_q vs. Real I_q [A], *Theta* [rad], I_r I_s I_t [A]

In the following test, a step I_q setpoint was introduced that varies between 0,4 A and -0,4 A. The objective was to observe a behavior similar to that of the test performed in the simulation. In this case, it was also decided to visualize and compare I_d to determine whether it was affected by the change in the current. Figure 46 shows that this is not the case; it even presents less noise than I_q.

Fig. 46 - Experimental Test 2: Setpoint I_q vs. Real I_q [A], Setpoint I_d vs. Real I_d [A]

Regarding the current, a behavior similar to the simulation was observed. As soon as the step is executed, the current suffers from some disturbances, although this does not invert its order. Similar to the simulation, the angle of rotation of the motor is also reversed. As shown in figure 47, at approximately 5,10 s, the order of the currents is inverted, although the direction of rotation of the motor (the angle) remains the same.

Fig. 47 - Experimental Test 2: I_r I_s I_t [A], *Theta* [rad]

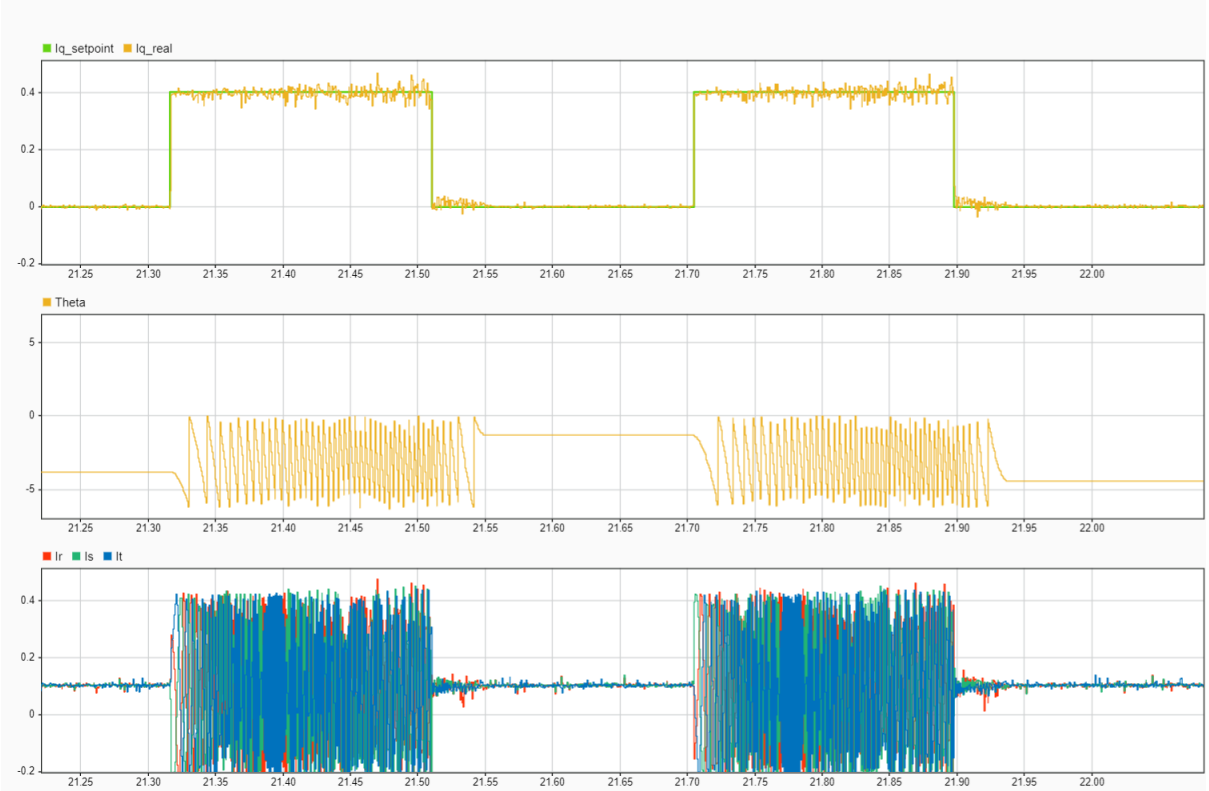

Fig. 48 - Experimental Test 3: Setpoint I_q vs. Real I_q [A], *Theta* [rad], I_r I_s I_t [A]

Finally, the third simulation test was performed by applying alternating I_q. Similar behavior to the simulation test was observed, although in this case, the scope shows the system in the stationary regime, so the currents were the same during the periods of activity (already saturated). In figure 48, it can be seen that the system has a short delay between I_q being set to 0 A and when the motor stops rotating. However, it is less than 0,1 s, so the control result is considered good.

In conclusion, because a very similar behavior was obtained in both simulation and experimental tests, both models are considered valid. The experimentation phase is completed successfully.

5. Economic study

This section examines the potential costs of the laboratory test experiment, such as the cost of equipment and materials, personnel costs, and any associated facility costs.

This study could also assess the potential benefits of the experiment, potential cost savings resulting from improved motor control, and the potential for intellectual property creation and patent applications. However, for this particular case it has not been taken into account, since it is dealing with a theoretical experiment of a thesis. In addition, it has performed with development kits which would not be used in real applications, so only the costs of carrying out the test are reflected.

The costs of the project are summarized in the following table, according to the software mentioned above and the hardware described in section 4.2.1. Hardware.

Material Description			**Cost**
Hardware			
AC motor		Industrial-Grade NEMA 23 Motor [16]	255,32 €/u
Microcontroller		LAUNCHXL-F28069M [17]	35,5 €/u
Three-phase inverter		BOOSTXL-DRV8305EV [18]	72 €/u
Power supply		AX-3003D AXIOMET [19]	133,98 €/u
Oscilloscope		PicoScope 2204A [20]	139 €/u
Cables and connectors			-
	Power supply cables	Test cable with connector 4 mm RS PRO [21]	5,97 €/u
Associated facility			
Test Laboratory			-
	Proteccion		-
Personnel			
12 ECTS at 30 h/ECTS		8,45 €/h (MIS)	3.042 €
Directors support - 30 h		8,45 €/h (MIS)	253,5 €

Software		
Matlab [22]		860 €/year
	Embedded Coder	1.300 €/year
	Embedded Coder Support Package for Texas Instruments C2000 Processors	860 €/year
	Fixed-Point Designer	1.300 €/year
	Matlab Coder	2.600 €/year
	Motor Control Blockset	860 €/year
	Optimization Toolbox	500 €/year
	Simulink	1.300 €/year
	Simulink Coder	1.300 €/year
	Simulink Design Optimization	500 €/year
	Simulink Desktop Real-Time	860 €/year
Code Composer Studio [23]	Integrated development environment (IDE) for TI's microcontrollers and processors	-
Pico Log [24]	Data logging software	-
Total cost		**15.795,76 €**
Total cost without Personnel and Software		**513,76 €**
Total cost of hardware*		**362,82 €**

Tab. 1 - Project cost detail

It has been decided to differentiate between the total cost of the material and the total cost including personnel and software licenses, since, for example, as it is a project in the academic field, there has been access to software licenses.

Besides, the hardware cost necessary to perform this project is 362,82 €, including the controller, inverter and motor. On the other hand, if the controller is performed for another motor, the test could be replicated with the cost of purchasing the *LAUNCHXL-F28069M* development kit and inverter. Even more, the implementation could be performed for other kits with similar characteristics, being able to use already available hardware, although it could require redoing partially or entirely the controller model.

6. Environmental implications

Advances in electric motor control technology have the potential to bring about significant environmental benefits, making this a crucial area of study. This section explores the environmental implications of advancements in motor control, focusing on their impacts on various industries, particularly the automotive sector. This research highlights several key topics that shed light on the positive environmental effects of advancements in motor control.

One significant aspect is the improvement in the performance and efficiency achieved through optimized control algorithms and precise sensor feedback. These advancements enable motors to operate at peak efficiency levels, minimize energy losses, and reduce overall power consumption. The enhanced efficiency translates into lower energy requirements, resulting in reduced carbon emissions and decreased reliance on fossil fuels.

Another important factor to consider is the reduction in energy consumption facilitated by the advanced motor control techniques. By implementing sophisticated control strategies, motors can adapt their operation based on real-time demand and adjust their power output to match the required load. This capability not only enhances energy efficiency, but also reduces unnecessary energy wastage during periods of low demand or idle states. Consequently, this leads to more sustainable use of resources and a reduced environmental footprint.

Furthermore, the extension of motor lifespan through effective control algorithms contributes to environmental sustainability. By mitigating common issues, such as overheating, voltage spikes, and mechanical stress, motor failures can be minimized. This reduction in motor replacement not only conserves resources but also reduces the waste generation associated with the disposal of old motors.

In the automotive sector, advances in motor control play a crucial role in the promotion of electric vehicles and transition away from internal combustion engines. By continually enhancing motor control algorithms, EV manufacturers can improve their driving experience, thereby making electric cars more attractive to consumers. This, in turn, can lead to increased adoption of EVs, resulting in a substantial reduction in greenhouse gas emissions and air pollution caused by conventional vehicles.

Moreover, advancements in motor control can contribute to improving the range and power management of electric cars. Optimal control algorithms allow for efficient utilization of battery power and extend the driving range of EVs. By intelligently managing the power flow and distribution within the vehicle's electrical system, motor control technology can maximize energy utilization and minimize wastage. This, coupled with ongoing developments in battery technology, can significantly enhance the viability and appeal of electric vehicles as sustainable transportation options.

Additionally, the impact of motor control technology extends beyond the vehicles themselves to the manufacturing processes within the automotive sector. Robotic arms, which are extensively used in automobile assembly lines, can benefit from enhanced motor-control algorithms. By improving the precision and efficiency of these robotic systems, motor control advancements can contribute to reducing errors, minimizing material waste, and optimizing production workflows. This, in turn, leads to more resource-efficient manufacturing processes and a reduced environmental impact.

Integrating electric motor control with renewable energy sources is another aspect worth considering. Electric motor control can facilitate efficient integration of renewable energy sources, such as solar and wind power, into the grid. By effectively managing the power flow between these sources and motors, renewable energy can be utilized more efficiently, reducing reliance on non-renewable energy and lowering greenhouse gas emissions.

Noise and vibration reduction are important environmental considerations. Advanced motor control techniques can help minimize the noise and vibration generated by electric motors, contributing to a more environmentally friendly and sustainable working and living environment.

In conclusion, the environmental implications of advances in electric motor control are significant. Improved performance and efficiency, reduced energy consumption, and increased motor lifespan contribute to a more sustainable use of resources. Moreover, these advancements have helped popularize electric cars, increase their range, and enhance their power management. Additionally, the impact extends to the manufacturing processes and optimizes the efficiency of robotic arms. These factors were considered, along with the integration of renewables.

7. Conclusions

In conclusion, this thesis on electric motor control provides valuable insights into the advancements and implications of motor control technology. This study encompassed both simulation and experimental tests, validating the effectiveness and reliability of the proposed control algorithms. By analyzing the simulation model and comparing it with the experimental results, it is evident that the developed control system exhibits similar behavior in both domains, reinforcing the validity and applicability of the model.

Simulation tests demonstrated the correct operation of the motor under different loads and setpoint variables. The response of the system to changes in the direction of rotation as well as cyclic setpoint currents was observed and analyzed. The simulation results indicate the effectiveness of the control parameters and the motor's ability to adapt to various operating conditions.

Experimental tests conducted using real hardware further confirm the simulation findings. Despite the limitations in signal quality owing to communication constraints, the experimental results showed consistent behavior comparable to that of the simulation tests. The step setpoint currents, direction reversal, and cyclic setpoint currents were successfully replicated in the experimental setup. These findings support the conclusion that the simulation model accurately represents a real world motor control system.

The economic study section highlights the potential costs associated with the test. The total cost of the project, considering personnel and software licenses, was also analyzed. This economic study provides a comprehensive overview of the financial aspects involved in conducting the experiment.

Furthermore, this thesis considers the environmental implications of advancements in motor-control technology. The research emphasized the positive effects of advancements in motor control on energy efficiency, reduced carbon emissions, and resource conservation. The optimized control algorithms and precise sensor feedback enabled the motors to operate at peak efficiency levels, resulting in reduced power consumption and environmental impact. The study also highlighted the potential for electric vehicle promotion, improved range and power management, and resource-efficient manufacturing processes through enhanced motor control.

This thesis has made contributions to the understanding and advancement of electric motor control technologies. The combination of simulation and experimental tests, along with economic and environmental analyses, provided a holistic view of the subject matter. The results and findings of this research have practical implications for various industries, particularly automotive applications and renewable energy integration.

To further enhance the control model and simulation, several improvements can be considered. First, incorporating heat models into the system would provide valuable insights into the thermal behavior and facilitate the optimization of cooling strategies. This addition would enable a more comprehensive analysis of the thermal performance of the motor, leading to improved reliability and efficiency. Furthermore, the integration of Kalman filters into the control model enhances the accuracy and reliability of sensor measurements. By effectively fusing sensor data with system dynamics, Kalman filters can provide precise estimates of motor states and variables, thereby enabling better control and monitoring of the system.

Another valuable enhancement would involve the inclusion of simulations of the external forces. By simulating real world conditions and external disturbances, the control model can be tested and refined in dynamic environments. Finally, exploring topics such as field devitalization and other suggested areas of research would expand the project's potential applications. By incorporating these topics into the project base, it becomes a versatile platform for the development of future projects and applications.

Overall, this thesis serves as a comprehensive guide for researchers, engineers, and industry professionals seeking to develop and implement effective motor-control systems. The validation of the simulation model through experimental tests and the consideration of economic and environmental aspects further enhances the relevance and applicability of the research. The findings presented in this thesis are expected to pave the way for future implementations and improve motor control techniques in projects such as Formula and Moto student.

8. Bibliographic references

[1] Shaohua Qiu, Xiaopeng Cui, Zuowei Ping ,Nanliang Shan, Zhong Li, Xianqiang Bao and Xinghua Xu. *Deep Learning Techniques in Intelligent Fault Diagnosis and Prognosis for Industrial Systems: A Review* [online]. National Key Laboratory of Science and Technology on Vessel Integrated Power System, Naval University of Engineering. 2023 [Consulted: February 15, 2023]. Available at: https://doi.org/10.3390/s23031305

[2] The MathWorks, Inc. *Parameter Tuning and Signal Logging with Serial Communication* [online]. 2023 [Consulted: February 27, 2023]. Available at: https://es.mathworks.com/help/ti-c2000/ug/parameter-tuning-external-mode.html

[3] The MathWorks, Inc. *Signal Logging and Parameter Tuning in XCP External Mode with Packed Mode* [online]. 2023 [Consulted: February 27, 2023]. Available at: https://es.mathworks.com/help/supportpkg/arduino/ref/packed-mode-example.html

[4] The MathWorks, Inc. *Open-Loop Control of 3-Phase AC Motors Using C2000 Processors* [online]. 2023 [Consulted: March 9, 2023]. Available at:https://es.mathworks.com/help/ti-c2000/ug/open-loop-c2000-example.html

[5] The MathWorks, Inc. *SVPWM Generator (2-Level)* [online]. 2023 [Consulted: March 17, 2023]. Available at: https://es.mathworks.com/help/sps/powersys/ref/svpwmgenerator2level.html?s_tid=srchtitle

[6] The MathWorks, Inc. *Control de campo orientado. Desarrolle algoritmos de control de campo orientado mediante la simulación* [online]. 2023 [Consulted: March 10, 2023]. Available at: https://es.mathworks.com/solutions/electrification/field-oriented-control.html

[7] The MathWorks, Inc. *Alpha-Beta-Zero to dq0, dq0 to Alpha-Beta-Zero* [online]. 2023 [Consulted: March 17, 2023]. Available at: https://es.mathworks.com/help/sps/powersys/ref/alphabetazerotodq0dq0toalphabetazero.html;jsessionid=e8c041f4a52424e7f228a9a0e447

[8] The MathWorks, Inc. *Six Step Commutation* [online]. 2023 [Consulted: March 17, 2023]. Available at: https://es.mathworks.com/help/mcb/ref/sixstepcommutation.html

[9] Hongjin Hu, Haoze Wang, Kun Liu ,Jingbo Wei and Xiangjie Shen. *A Simplified Space Vector Pulse Width Modulation Algorithm of a High-Speed Permanent Magnet Synchronous Machine Drive for a Flywheel Energy Storage System* [online]. School of Aeronautics and Astronautics, Sun Yat-Sen University, 2022 [Consulted: February 22, 2023]. Available at: https://doi.org/10.3390/en15114065

[10] Bergas Jané, Joan. *Control del motor d'inducció considerant els límits del convertidor i del motor* [online]. Doctoral thesis, UPC, Departament d'Enginyeria Elèctrica, 2000 [Consulted: February 10, 2023]. Available at: http://hdl.handle.net/10803/6293

[11] The MathWorks, Inc. *C2802x/C2803x/C2805x/C2806x/F28M3x/F2807x/F2837xD/F2837xS/F2838x/F28004x/F28002x/F28003x ADC* [online]. 2023 [Consulted: April 12, 2023]. Available at: https://es.mathworks.com/help/ti-c2000/ref/c2802xc2803xc2805xc2806xf28m3xf2807xf2837xdf2837xsf2838xf28004xf28002xf28003xadc.html

[12] Texas Instruments. BOOSTXL-DRV8305EVM User's Guide [online]. Manufacturer's manual/ datasheet, 2017 [Consulted: March 3, 2023]. Available at: https://www.ti.com/lit/ug/slvuai8a/slvuai8a.pdf?ts=1632391080279&ref_url=https%253A%252F%252Fwww.ti.com%252Ftool%252FBOOSTXL-DRV8305EVM

[13] The MathWorks, Inc. *c280x/C2802x/C2803x/C2805x/C2806x/C2833x/C2834x/F28M3x/F2807x/F2837xD/F2837xS/F2838x/F28004x/F28002x/F28003x ePWM ADC* [online]. 2023 [Consulted: April 12, 2023]. Available at: https://es.mathworks.com/help/ti-c2000/ref/c280xc2802xc2803xc2805xc2806xc2833xc2834xf28m3xf2807xf2837xdf2837xsf2838xf28004xf28002xf28003xepwm.html

[14] Teknic. Industrial-Grade NEMA 23 Motors [online]. Manufacturer's manual/ datasheet [Consulted: March 3, 2023]. Available at:https://www.teknic.com/files/product_info/N23_Industrial_Grade_Motors.pdf

[15] Texas Instruments. LAUNCHXL-F28069M Overview [online]. Manufacturer's manual/ datasheet, 2019 [Consulted: March 3, 2023]. Available at: https://www.ti.com/lit/ug/sprui11b/sprui11b.pdf?ts=1631779978788&ref_url=https%253A%252F%252Fwww.ti.com%252Ftool%252FLAUNCHXL-F28069M

[16] Teknic. *HUDSON BRUSHLESS MOTOR SELECTION* [online]. 2023 [Consulted: April 6, 2023]. Available at: https://teknic.com/products/brushless-servo-motors/hudson-motors-ready-ship/

[17] Texas Instruments. *LAUNCHXL-F28069M, F28069M LaunchPad™ development kit for C2000™ Piccolo™ MCU* [online]. 2023 [Consulted: April 6, 2023]. Available at: https://www.ti.com/tool/LAUNCHXL-F28069M

[18] Texas Instruments. *BOOSTXL-DRV8305EVM, DRV8305N 3-Phase Motor Drive BoosterPack Evaluation Module* [online]. 2023 [Consulted: April 6, 2023]. Available at: https://www.ti.com/product/BOOSTXL-DRV8305EVM/part-details/BOOSTXL-DRV8305EVM

[19] Texas Instruments. *BOOSTXL-DRV8305EVM, DRV8305N 3-Phase Motor Drive BoosterPack Evaluation Module* [online]. 2023 [Consulted: April 6, 2023]. Available at: https://www.tme.eu/es/details/ax-3003d/alimentadores-monocanales/axiomet/?brutto=1&currency=EUR

[20] Pico Technology. *PicoScope® 2000 Series, Like a benchtop oscilloscope, only smaller and better* [online]. 2023 [Consulted: April 6, 2023]. Available at: https://www.picotech.com/oscilloscope/2000/picoscope-2000-overview

[21] RS PRO. *Cable de prueba con conector de 4 mm RS PRO de color Rojo, Macho-Macho, 50V ac, 2.5A, 1m* [online]. 2023 [Consulted: April 6, 2023]. Available at: https://es.rs-online.com/web/p/cables-de-prueba/6684588

[22] The MathWorks, Inc. *MATLAB Pricing and Licensing* [online]. 2023 [Consulted: April 6, 2023]. Available at: https://es.mathworks.com/pricing-licensing.html

[23] Texas Instruments. *CCSTUDIO, Code Composer Studio™ integrated development environment (IDE)* [online]. 2023 [Consulted: April 6, 2023]. Available at: https://www.ti.com/tool/CCSTUDIO

[24] Pico Technology. *PicoLog 6 data logging software* [online]. 2023 [Consulted: April 6, 2023]. Available at: https://www.picotech.com/library/data-loggers/picolog-6-data-logger-software

[25] Bergas Jané, Joan. *Obtenció de l'equació de les tensions del motor brushless.* Apunts Maple, UPC, Departament d'Enginyeria Elèctrica, 2023.

9. Annex

9.1. Annex 1: PMSM mathematical model

Obtaining the equation of the voltages of the brushless motor

To obtain the equation that describes the behavior of the brushless motor, it will hang as a representation of the same, which is shown in the attached figure.

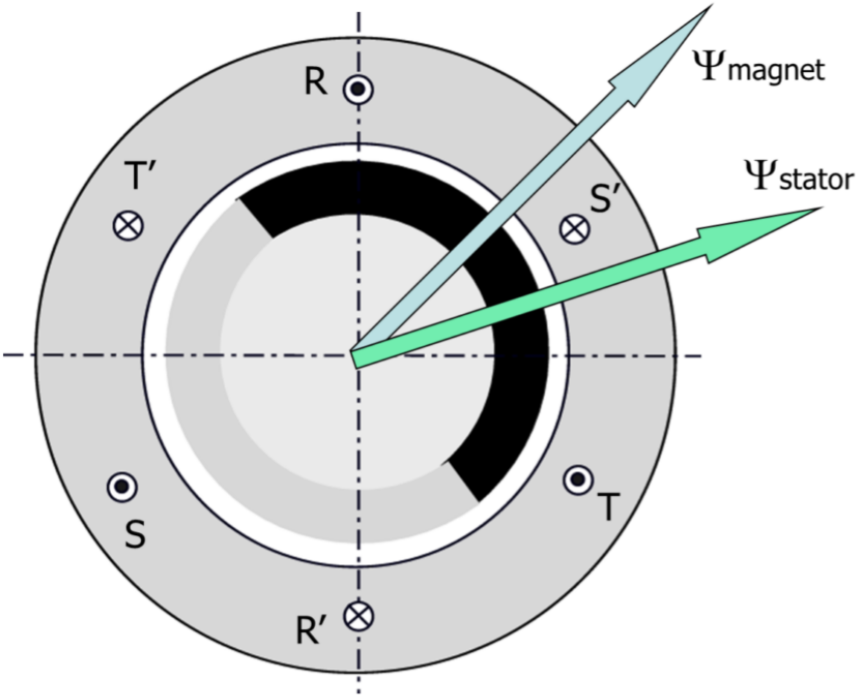

Fig. 49 - Brushless motor representation [25]

$$\begin{bmatrix}\varphi_r\\ \varphi_s\\ \varphi_t\end{bmatrix} = \begin{bmatrix} M & M\cdot\cos\left(\frac{2\pi}{3}\right) & M\cdot\cos\left(\frac{-2\pi}{3}\right)\\ M\cdot\cos\left(\frac{-2\pi}{3}\right) & M & M\cdot\cos\left(\frac{2\pi}{3}\right)\\ M\cdot\cos\left(\frac{2\pi}{3}\right) & M\cdot\cos\left(\frac{-2\pi}{3}\right) & M\end{bmatrix}\cdot\begin{bmatrix}i_r\\ i_s\\ i_t\end{bmatrix} + \begin{bmatrix}\psi\cdot\cos(\alpha)\\ \psi\cdot\cos\left(\alpha+\frac{2\pi}{3}\right)\\ \psi\cdot\cos\left(\alpha-\frac{2\pi}{3}\right)\end{bmatrix}$$

Note: α is the position angle of the rotor magnetic field.

$$\begin{bmatrix}\varphi_r\\ \varphi_s\\ \varphi_t\end{bmatrix} = \begin{bmatrix} M & -\frac{1}{2}M & -\frac{1}{2}M\\ -\frac{1}{2}M & M & -\frac{1}{2}M\\ -\frac{1}{2}M & -\frac{1}{2}M & M\end{bmatrix}\cdot\begin{bmatrix}i_r\\ i_s\\ i_t\end{bmatrix} + \begin{bmatrix}\psi\cdot\cos(\alpha)\\ \psi\cdot\cos\left(\alpha+\frac{2\pi}{3}\right)\\ \psi\cdot\cos\left(\alpha-\frac{2\pi}{3}\right)\end{bmatrix}$$

The stray flux of the stator windings was then introduced.

$$\begin{bmatrix} v_r \\ v_s \\ v_t \end{bmatrix} = \begin{bmatrix} R_s & 0 & 0 \\ 0 & R_s & 0 \\ 0 & 0 & R_s \end{bmatrix} \cdot \begin{bmatrix} i_r \\ i_s \\ i_t \end{bmatrix} + \frac{d}{dt} \left(\begin{bmatrix} L_{sd}+M & -\frac{1}{2}M & -\frac{1}{2}M \\ -\frac{1}{2}M & L_{sd}+M & -\frac{1}{2}M \\ -\frac{1}{2}M & -\frac{1}{2}M & L_{sd}+M \end{bmatrix} \cdot \begin{bmatrix} i_r \\ i_s \\ i_t \end{bmatrix} + \begin{bmatrix} \psi \cdot \cos(\alpha) \\ \psi \cdot \cos\left(\alpha + \frac{2\pi}{3}\right) \\ \psi \cdot \cos\left(\alpha - \frac{2\pi}{3}\right) \end{bmatrix} \right)$$

Equation of stresses in an arbitrary reference.

The equation obtained in the previous section is expressed in the reference *abc*, and is almost intractable, since it is a system of 3 differential equations, with non-constant coefficients. To remedy the previous problems, the previous equation expressed in the base *abc* must be transformed into another base where the coefficients become constant or at least non-linear (in the previous equation, terms with cosine and sine appeared).

Therefore, Park's transformation is applied, a transformation that is represented by its matrix defined below. To apply Park's transformation to the previous equation, proceed as shown:

Initially the stress equation in matrix form is defined:

$$V = RI + \frac{d}{dt}(MI + \Psi)$$

Considering that the stator coupling matrix is constant, can be express as:

$$V = RI + M\frac{d}{dt}I + \frac{d}{dt}\Psi$$

If now P is defined as the *Park matrix*, and multiply the previous equation by this matrix (and enter the identity matrix as $P \cdot P^{-1}$), is obtained:

$$PV = PRP^{-1}PI + PM\frac{d}{dt}(P^{-1}PI) + P\frac{d}{dt}\Psi$$

Then, if $V_p = PV$ and $I_p = PI$ are defined and take into account that $P{\cdot}R{\cdot}P^{-1} = R$ (since $R = Rs{\cdot}I$, where I is the identity matrix):

$$V_p = RI_p + PM\frac{d}{dt}(P^{-1})I_p + PMP^{-1}\frac{d}{dt}(I_p) + P\frac{d}{dt}\Psi$$

Mathematical operations

$$Park\,Matrix = \begin{bmatrix} \frac{1}{6}\sqrt{6}\sqrt{2} & \frac{1}{6}\sqrt{6}\sqrt{2} & \frac{1}{6}\sqrt{6}\sqrt{2} \\ \frac{1}{3}\sqrt{6}\cos(\alpha) & -\frac{1}{3}\sqrt{6}\cos\left(\alpha + \frac{1}{3}\pi\right) & -\frac{1}{3}\sqrt{6}\cos\left(\alpha + \frac{1}{6}\pi\right) \\ -\frac{1}{3}\sqrt{6}\cos(\alpha) & \frac{1}{3}\sqrt{6}\cos\left(\alpha + \frac{1}{3}\pi\right) & -\frac{1}{3}\sqrt{6}\cos\left(\alpha + \frac{1}{6}\pi\right) \end{bmatrix}$$

$$Resistances\ Matrix = \begin{bmatrix} Rs & 0 & 0 \\ 0 & Rs & 0 \\ 0 & 0 & Rs \end{bmatrix}$$

$$Couplings\ Matrix = \begin{bmatrix} L_{ds} + M & -\frac{1}{2}M & -\frac{1}{2}M \\ -\frac{1}{2}M & L_{ds} + M & -\frac{1}{2}M \\ -\frac{1}{2}M & -\frac{1}{2}M & L_{ds} + M \end{bmatrix}$$

$$Rotor\ Flow = \begin{bmatrix} \psi \cdot \cos\left(\alpha + \alpha_0\right) \\ -\psi \cdot \cos\left(\alpha + \alpha_0 + \frac{1\pi}{3}\right) \\ -\psi \cdot sin\left(\alpha + \alpha_0 + \frac{1\pi}{6}\right) \end{bmatrix}$$

$$Couplings\ Matrix\ Der = \begin{bmatrix} 0 & 0 & 0 \\ 0 & 0 & 0 \\ 0 & 0 & 0 \end{bmatrix}$$

$$Park\ Matrix\ Der = \begin{bmatrix} 0 & 0 & 0 \\ -\frac{1}{3}\, w_m \sqrt{6}\, \sin\left(\alpha\right) & \frac{1}{3}\, w_m \sqrt{6}\, \sin\left(\alpha + \frac{1}{3}\pi\right) & -\frac{1}{3}\, w_m \sqrt{6}\, \sin\left(\alpha + \frac{1}{6}\pi\right) \\ -\frac{1}{3}\, w_m \sqrt{6}\, \sin\left(\alpha\right) & \frac{1}{3}\, w_m \sqrt{6}\, \sin\left(\alpha + \frac{1}{3}\pi\right) & -\frac{1}{3}\, w_m \sqrt{6}\, \sin\left(\alpha + \frac{1}{6}\pi\right) \end{bmatrix}$$

$$Rotor\ Flow\ Der = \begin{bmatrix} -w_m\, \psi\, \cos\left(\alpha + \alpha_0\right) \\ w_m\, \psi\, sin\left(\alpha + \alpha_0 + \frac{1}{3}\pi\right) \\ -w_m\, \psi\, cos\left(\alpha + \alpha_0 + \frac{1}{6}\pi\right) \end{bmatrix}$$

$$PM\frac{d}{dt}(P-1) = \begin{bmatrix} 0 & 0 & 0 \\ 0 & 0 & -\frac{1}{2}w_m(2L_{ds} + 3M) \\ 0 & \frac{1}{2}w_m(2L_{ds} + 3M) & 0 \end{bmatrix}$$

$$PMP^{-1} = \begin{bmatrix} L_{ds} & 0 & 0 \\ 0 & L_{ds} + \frac{3}{2}M & 0 \\ 0 & 0 & L_{ds} + \frac{3}{2}M \end{bmatrix}$$

For simplicity, it is assumed that the Park transform is well oriented; therefore, $\alpha_0 = 0$:

$$\begin{bmatrix} -w_m\,\psi\,sin(\alpha+\alpha_0) \\ w_m\,\psi\;sin\left(\alpha+\alpha_0+\frac{1}{3}\pi\right) \\ -w_m\,\psi\;cos\left(\alpha+\alpha_0+\frac{1}{6}\pi\right) \end{bmatrix}$$

$$Sum\,Matrices = \begin{bmatrix} L_{ds}\,p+Rs & 0 & 0 \\ 0 & Rs+p\left(L_{ds}+\frac{3}{2}M\right) & -\frac{1}{2}w_m(2L_{ds}+3M) \\ 0 & \frac{1}{2}w_m(2L_{ds}+3M) & Rs+p\left(L_{ds}+\frac{3}{2}M\right) \end{bmatrix}$$

If all homopolar components are removed, because the machine has an isolated neutral, the sum of the three intensities of the stator is zero:

$$Matrix\,V = \begin{bmatrix} Rs+p\left(L_{sd}+\frac{3}{2}M\right) & \frac{-1}{2}w_m\cdot(2L_{ds}+3M) \\ \frac{1}{2}w_m\cdot(2L_{ds}+3M) & Rs+p\left(L_{sd}+\frac{3}{2}M\right) \end{bmatrix}$$

Once all the previous operations have been carried out, the equation that describes the behavior of the induction motor in a transient regime is obtained as follows:

$$V_p = MatrixV\cdot I_p + \lambda$$

Where MatrixV is described above. The rotor flux matrix is defined as follows:.

$$Rotor\,Flux\,Matrix = \begin{bmatrix} 0 \\ 0 \\ \frac{1}{2}\sqrt{6}\;w_m\,\psi \end{bmatrix}$$

State space

From the previous section, the total inductance of the stator is defined as *Ls = Lds + M*, which simplifies the resulting system:

$$\begin{bmatrix} V_d \\ V_q \end{bmatrix} = \begin{bmatrix} R_s & -w\cdot L_s \\ w\cdot L_s & R_s \end{bmatrix}\begin{bmatrix} I_d \\ I_q \end{bmatrix} + \begin{bmatrix} L_s & 0 \\ 0 & L_s \end{bmatrix}\frac{d}{dt}\begin{bmatrix} I_d \\ I_q \end{bmatrix} + \begin{bmatrix} 0 \\ \sqrt{\frac{3}{2}}\,w_m\,\psi \end{bmatrix}$$

If the term with derivatives is isolated, the equation of state is obtained as:

$$\frac{d}{dt}\begin{bmatrix} I_d \\ I_q \end{bmatrix} = \begin{bmatrix} -\frac{R_s}{L_s} & w \\ -w & -\frac{R_s}{L_s} \end{bmatrix}\begin{bmatrix} I_d \\ I_q \end{bmatrix} + \begin{bmatrix} \frac{1}{L_s} & 0 \\ 0 & \frac{1}{L_s} \end{bmatrix}\begin{bmatrix} V_d \\ V_q \end{bmatrix} + \begin{bmatrix} 0 \\ k_\varphi\cdot w_m \end{bmatrix}$$

Torque of the brushless motor

To determine the torque of the brushless motor, the following expression, obtained from the electromechanical conversion, is applied:

$$\Gamma(t) = \frac{1}{2}[i]^t \frac{d}{d\alpha}[M(\alpha)][i]$$

It will be assumed that in the rotor we have a field created by an inductance such that

$$\varphi_r = \psi = M \cdot I_{iman}$$

Therefore, the coupling matrix is obtained as follows:.

$$\begin{bmatrix} \varphi_r \\ \varphi_s \\ \varphi_t \\ \varphi_{iman} \end{bmatrix} = \begin{bmatrix} M & -\frac{1}{2}M & -\frac{1}{2}M & M \cdot \cos(\alpha) \\ -\frac{1}{2}M & M & -\frac{1}{2}M & M \cdot \cos\left(\alpha - \frac{2\pi}{3}\right) \\ -\frac{1}{2}M & -\frac{1}{2}M & M & M \cdot \cos\left(\alpha + \frac{2\pi}{3}\right) \\ M \cdot \cos(\alpha) & M \cdot \cos\left(\alpha - \frac{2\pi}{3}\right) & M \cdot \cos\left(\alpha + \frac{2\pi}{3}\right) & L_{iman} \end{bmatrix} \cdot \begin{bmatrix} i_r \\ i_s \\ i_t \\ i_{iman} \end{bmatrix}$$

Once operated, the torque expression is:

$$\Gamma(t) = M \cdot i_{iman}\left(-i_r \cdot \sin(\alpha) - i_s \cdot \sin\left(\alpha - \frac{2\pi}{3}\right) - i_t \cdot \sin\left(\alpha + \frac{2\pi}{3}\right)\right)$$

This expression can be easily verified to be equivalent to

$$\Gamma(t) = \varphi \cdot I_q$$